Department of Physics and Astronomy
University of Heidelberg

Discovery potential of the Two-Higgs-Doublet Model with Maximal CP Symmetry with the ATLAS experiment

Bachelor Thesis in Physics
submitted by

Philipp Pigard

born in Eberswalde-Finow (Germany)

2012

This Bachelor Thesis has been carried out by Philipp Pigard at the
Kirchhoff-Institute for Physics in Heidelberg
under the supervision of
Prof. Dr. Hans-Christian Schultz-Coulon

Abstract

Presented in this thesis is a sensitivity study for a search of the Two-Higgs-Doublet Model with maximal CP symmetry (MCPM) [16] at the ATLAS experiment of the LHC. Starting from the implementation of the MCPM into the Monte Carlo event generator MadGraph [6], a full Monte Carlo simulation chain including the fast detector simulation Atlfastii-D was implemented and extended for the use on the LHC computing grid. Based on an existing particle search at ATLAS, the Standard Model background and the simulated MCPM signal were processed through an event selection written in C++. The excess over Standard Model background is quantified and the luminosities needed for discovery and exclusion are estimated. For MCPM Higgs masses $m_{h'}$ smaller than 200 GeV the total luminosity to be collected in 2012 will suffice to exclude the MCPM hypothesis if no excess is found. Finally, two optimizations to the event selection based on the event topologies of MCPM signal and Standard Model background are discussed. The developed Monte Carlo MCPM signal generation chain and the event selection will be suitable for future MCPM searches.

Zusammenfassung

In dieser Arbeit wird das Entdeckungspotential des Zwei-Higgs-Doublet-Modells mit maximaler CP-Symmetrie (MCPM) [16] durch das ATLAS Experiments am LHC untersucht. Ausgehend von der Implementierung des MCPM in die Monte-Carlo-Simulation MadGraph [6] wurde eine vollständige Monte-Carlo-Simulation der MCPM-Ereignisse entwickelt. Das zu erwartende Detektorsignal wurde mit der schnellen Detektorsimulation Altlast ii-D simuliert. Anschließend wurden die Ereignis- und Detektorsimulation für die Verwendung auf dem LHC-Computergrid angepasst. Basierend auf einer bestehenden ATLAS-Analyse wurden der Untergrund durch Physikprozesse des Standardmodells und das simulierte MCPM-Signal durch eine in C++ programmierte Ereignisselektion für weitere Analysen vorbereitet. Die durch MCPM-Prozesse gegenüber dem Standardmodell erhöhten Ereigniszahlen wurden verwendet, um die notwendigen Luminositäten für eine Entdeckung beziehungsweise den Ausschluss des MCPMs abzuschätzen. Für Higgsmassen $m_{h'}$ kleiner als 200 GeV würde die für 2012 angestrebte Gesamtluminosität für den Ausschluss der MCPM-Hypothese ausreichen. Abschliessend wurden zwei Möglichkeiten zur Verbesserung der Ereignisselektion anhand der Zerfallseigenschaften des Standardmodell-Untergrunds und des MCPM-Signals diskutiert. Die im Rahmen dieser Arbeit implementierte Ereignissimulation und -selektion sind nach Anpassungen für eine zukünftige MCPM-Analyse geeignet.

Contents

1 The Standard Model of particle physics **6**

2 The Two-Higgs-Doublet Model with maximal CP symmetry **8**

3 MCPM Signal and SM background **10**

4 The ATLAS experiment at the LHC **14**
4.1 The Large Hadron Collider 14
4.2 The ATLAS detector 15

5 Monte Carlo event generation **18**
5.1 MCPM signal definition and simulation chain 19
5.2 Bare event generation with MadGraph 20
5.3 Event generation with Pythia 23
5.4 Detector simulation - Atlfast II 25

6 Background simulation **29**

7 Dimuon resonance analysis **30**
7.1 Physics objects definitions 30
7.2 Event selection 30

8 Estimate of the discovery potential **35**

9 Summary **40**

A MCP analysis guideline **41**

B Results of the Breit-Wigner fits **42**

C SM background samples **43**

D Signal sample generation code **45**

E Bibliography **50**

Acknowledgements **51**

1 The Standard Model of particle physics

The Standard Model of particle physics (SM) is currently the best description of particle physics phenomena observed in nature. Originally developed during the 1970s, this quantum field theory has been tested thoroughly during the past 40 years and has predicted the existence and properties of the gauge bosons of the weak force, the top quark and the gluons of the strong force [19]. With the exception of gravity, the theory incorporates all known forces (electromagnetic, weak and strong) and particles into a remarkably simple theoretical framework.

The particles of the SM are commonly classified by their spin. Spin refers to the Lorentz transformation properties of the fields whose excitations are interpreted as particles. Particles of spin-½ are fermions and obey the Pauli principle, i.e. no physical state may be occupied by more than one fermion. The fermions of the SM are grouped into so-called families or generations, where only the fermions of the first generation are stable and the particle masses increase with each generation. All fermions of the SM, the generation ordering and the couplings to the interactions are shown in table 1.1. The interactions of the fermions are described by gauge fields which are derived by extending existing symmetries in the Lagrangian description of the theory. The resulting interaction fields are bosonic, meaning they carry integer spin.

The interactions of the SM, their mediator particles, the effective range of the interaction and the coupling strength relative to the strong force are shown in table 1.2, in which gravity is also included for comparison.

The success of the Standard Model as a description of particle physics phenomena observed in nature is undoubted, but experimental observations, e.g. from cosmology reveal problems that cannot be explained by the SM:

- observed gravitational effects cannot be explained solely by the presence of the visible matter (dark matter and dark energy problem)
- neutrino oscillations are not possible with the massless neutrinos of the SM [23]

Apart from experimental issues, there are theoretical aspects that suggest that there might be a physics theory beyond the SM.

Generation	Fermion	Mass	Charge	Couplings	
				Gauge	Higgs
1	u	$2.3\,\text{MeV} \approx 1.3 \cdot 10^{-5} m_t$	⅔	$g, \text{W}^{\pm}, \text{Z}, \gamma$	ρ
	d	$4.80\,\text{MeV} \approx 1.1 \cdot 10^{-3} m_b$	-⅓	$g, \text{W}^{\pm}, \text{Z}, \gamma$	ρ
	e	$0.51\,\text{MeV} \approx 2.9 \cdot 10^{-4} m_\tau$	-1	$\text{W}^{\pm}, \text{Z}, \gamma$	ρ
	ν_e	$< 2\,\text{eV}$	0	$\text{W}^{\pm}, \text{Z}$	–
2	c	$1.275\,\text{GeV} \approx 5.9 \cdot 10^{-2} m_t$	⅔	$g, \text{W}^{\pm}, \text{Z}, \gamma$	ρ
	s	$95\,\text{MeV} \approx 2.4 \cdot 10^{-2} m_b$	-⅓	$g, \text{W}^{\pm}, \text{Z}, \gamma$	ρ
	μ	$105.7\,\text{MeV} \approx 5.4 \cdot 10^{-2} m_\tau$	-1	$\text{W}^{\pm}, \text{Z}, \gamma$	ρ
	ν_μ	$< 2\,\text{eV}$	0	$\text{W}^{\pm}, \text{Z}$	-
3	t	$173.5\,\text{GeV}$	⅔	$g, \text{W}^{\pm}, \text{Z}, \gamma$	ρ
	b	$4.18\,\text{GeV}$	-⅓	$g, \text{W}^{\pm}, \text{Z}, \gamma$	ρ
	τ	$1.78\,\text{GeV}$	-1	$\text{W}^{\pm}, \text{Z}, \gamma$	ρ
	ν_τ	$< 2\,\text{eV}$	0	$\text{W}^{\pm}, \text{Z}$	-

Table 1.1: Particle content of the Standard Model including key physics properties and the couplings. The masses of the fermions have also been expressed in units of the corresponding 3rd generation particle to highlight the mass ordering. Charges are in units of e. All values from [15].

force	mediator	effective range	strength
strong	gluon g	1 fm	1
em	photon γ	∞	10^{-2}
weak	$\text{W}^{\pm}, \text{Z}$	10^{-18} m	10^{-7}
gravity	–	∞	10^{-39}

Table 1.2: The fundamental forces. The effective coupling strengths are normalized to the strong force. Gravity is not described in the framework of SM and no commonly agreed upon quantized theory of gravity exists.

2 The Two-Higgs-Doublet Model with maximal CP symmetry

In addition to the observations mentioned in the previous chapter, the SM with its 19 numerical parameters [18] poses plenty of unsolved problems and issues regarding the very structure of the theory. Some of these concerns are [6]:

- the number of fermion families is not uniquely determined by constraints within the theory
- the mass hierarchy of fermions is not a consequence of the theory
- the theory does not explain why the Cabibbo-Kobayashi-Maskawa (CKM) matrix is close to unity

These and other issues have inspired vivid research in constructing extensions to the SM. The Two-Higgs-Doublet-Model (THDM) is one of these extensions which postulates the existence of an additional scalar doublet. By requiring invariance under so-called generalized CP transformations, compelling theories may be constructed [17]. This thesis studies one specific THDM with a special symmetry under generalized CP transformations, it will be referred to as maximally CP symmetric model (MCPM) and its definition is given in [17]. The number of free parameters of the MCPM is 11, not counting representation assignments.

The MCPM has the same field content as the SM, except for the Higgs sector. There are five Higgs bosons in the MCPM: one uncharged particle ρ', which behaves very close to the Higgs predicted by the SM, two uncharged Higgs particles h' and h'' and two charged particles H^+ and H^-. The particle content of the MCPM and the coupling of the particles to the gauge and Higgs fields is shown in table 2.1.

In the MCPM, all shortcomings of the SM mentioned above are addressed and are predicted as a consequence of the theory, without any additional assumptions:

- the number of fermion families has to be at least two if fermions are to get masses
- the first and second fermion family remain massless, only the third fermion family obtains masses
- the CKM matrix is unity

Generation	Fermion	Mass	Charge	Couplings	
				Gauge	Higgs
1	u	0	$\frac{2}{3}$	$g, \mathrm{W}^{\pm}, \mathrm{Z}, \gamma$	-
	d	0	$-\frac{1}{3}$	$g, \mathrm{W}^{\pm}, \mathrm{Z}, \gamma$	-
	e	0	-1	$\mathrm{W}^{\pm}, \mathrm{Z}, \gamma$	-
	ν_e	0	0	$\mathrm{W}^{\pm}, \mathrm{Z}$	-
2	c	0	$\frac{2}{3}$	$g, \mathrm{W}^{\pm}, \mathrm{Z}, \gamma$	$h', h'', H^{\pm}$
	s	0	$-\frac{1}{3}$	$g, \mathrm{W}^{\pm}, \mathrm{Z}, \gamma$	$h', h'', H^{\pm}$
	μ	0	-1	$\mathrm{W}^{\pm}, \mathrm{Z}, \gamma$	$h', h'', H^{\pm}$
	ν_μ	0	0	$\mathrm{W}^{\pm}, \mathrm{Z}$	$h', h'', H^{\pm}$
3	t	m_t	$\frac{2}{3}$	$g, \mathrm{W}^{\pm}, \mathrm{Z}, \gamma$	ρ'
	b	m_b	$-\frac{1}{3}$	$g, \mathrm{W}^{\pm}, \mathrm{Z}, \gamma$	ρ'
	τ	m_τ	-1	$\mathrm{W}^{\pm}, \mathrm{Z}, \gamma$	ρ'
	ν_τ	0	0	$\mathrm{W}^{\pm}, \mathrm{Z}$	ρ'

Table 2.1: Particle content of the MCPM including key physics properties and the couplings. Charges are in units of e. Table source: [6].

Despite the experimental evidence of non-zero first and second fermion family masses and the off-diagonal CKM matrix elements, the MCPM might be an approximation and the underlying generalized CP transformations may serve as approximate symmetries of nature. The phenomenology of the MCPM at the LHC has been developed in [16].

This thesis studies the discovery potential of the MCPM with the ATLAS experiment via the increased cross section in the dimuon final state due to $h' \rightarrow \mu^+\mu^-$ decays. The Monte Carlo software implementation of the MCPM presented in [6] is embedded into a full Monte Carlo event generation. The ATLAS fast detector simulation is then employed to obtain the expected detector response due to these events. Standard Model background processes for the dimuon final state and the MCPM signal are processed by an event selection to estimate the possible discrimination of the background. Finally, the discovery potential of the MCPM is estimated by determining the luminosities necessary for discovery or exclusion.

3 MCPM Signal and SM background

This analysis of the MCPM discovery potential uses the muonic decay channel of the h'-Higgs despite the dominant decay modes being quark-antiquark and gluon-gluon processes [16]:

$$\frac{\sigma(h' \to \mu^+ + \mu^-)}{\sigma(\text{total})} \approx 10^{-5}. \tag{3.1}$$

Experimentally, the leptonic decay channel is easier to handle compared to hadronic processes. The QCD background cross section is at least eight orders of magnitude larger than the cross section times branching ratio of the Higgs decaying into pairs of $s\bar{s}$ and $c\bar{c}$ quarks [16, 20]. The determination of the flavor of the quark causing a jet, so-called jet tagging, is difficult and introduces considerable systematic uncertainties. Another systematic problem of the hadronic measurements are the jet energy scale (JES) uncertainties which would translate into a large systematic uncertainty on the reconstructed Higgs mass. Altogether, the muonic decay channel is the more promising one for the search for the neutral MCPM Higgs bosons. The cross section for the production and decay of either neutral MCPM Higgs boson h' or h'' is mass dependent and amounts to about 0.05 pb for masses of a few hundred GeV at $\sqrt{s} = 7$ TeV.

Figure 3.1 shows the measured production cross sections for the production of the Z, $t\bar{t}$ and diboson backgrounds from which a first estimate of the magnitude and hierarchy of backgrounds can be made. The SM background with the same dimuon final state is dominated by the muonic Drell-Yan process shown in figure 3.2. The total cross section of the Drell-Yan process is about 800 pb at $\sqrt{s} = 7$ TeV. In the context of this work, the term Drell-Yan always refers to the Drell-Yan process with muonic final state. The second largest background contribution comes from decays withinvolving $t\bar{t}$ intermediate states as shown in figure 3.3, which also shows the leading order production diagrams.

Background from processes involving two bosons of the weak force is also present. The leading order production processes are shown in figures 3.4 and 3.5. The leading order decay diagrams are shown in figure 3.6. Those processes contribute to the background because of limited geometric acceptance or failed reconstruction of muons. If, for example, one of the final state μ^+ in the decay $\mathrm{W^+Z} \to \mu^+\nu\mu^+\mu^-$ is not detected due to the limited geometric acceptance of the detector, the event will have the same particle content as the signal (see figure 3.7). An analysis of the missing transverse energy E_T^{miss} of the event would allow to deduce the existence of a undetected neutrino, but would also introduce a systematic uncertainty of the E_T^{miss} calculation. Considering the sufficient suppression of the diboson background without such an analysis, no further event

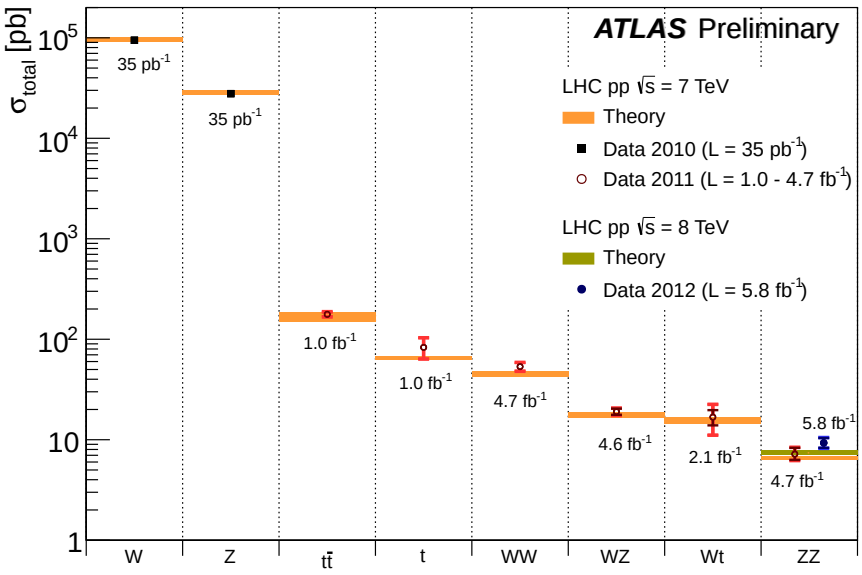

Figure 3.1: Measured total production cross sections for various processes including the background relevant for this study. The branching ratios for the dimuon final state are not taken into account. Image source: official ATLAS plot for ICHEP 2012.

selection based on E_T^{miss} considerations is employed in this study.

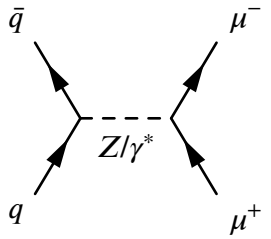

Figure 3.2: Feynman diagram of the Drell-Yan process

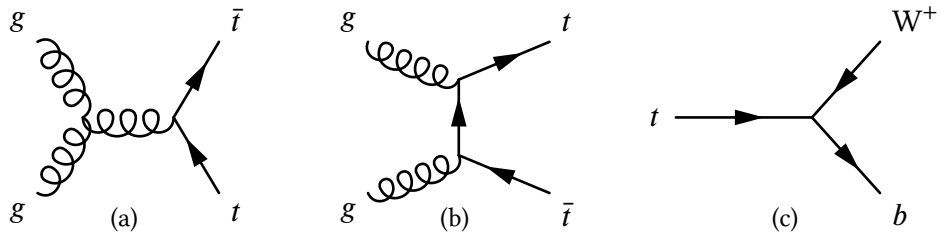

Figure 3.3: Leading order Feynman diagrams for $t\bar{t}$ production (a) and (b). Feynman diagram (c) shows the leading order process of a t decaying into W$^+$.

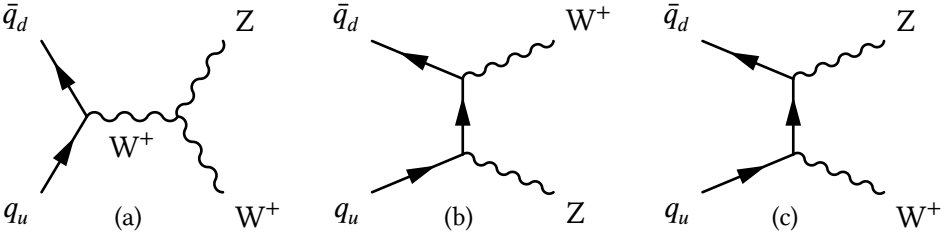

Figure 3.4: Tree level Feynman diagrams of W$^+$Z production. The indices u and d indicate up and down-type quarks respectively. The diagrams for W$^-$Z production are obtained by exchanging u and d in diagram (a) and by replacing quarks with antiquarks and vice versa in diagrams (b) and (c).

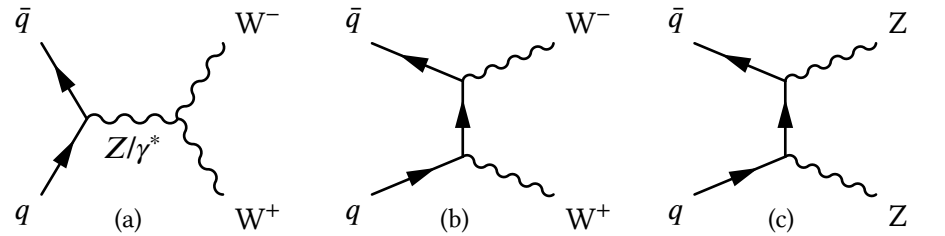

Figure 3.5: Tree level Feynman diagrams for W$^+$W$^-$ (a and b) and ZZ production (c).

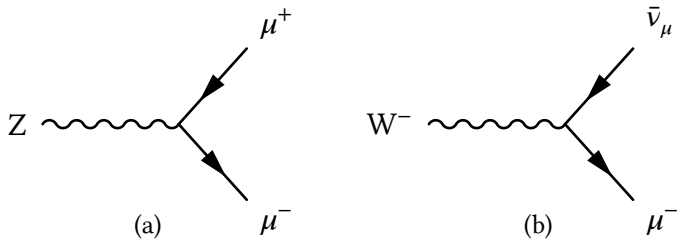

Figure 3.6: Tree level Feynman diagrams for (a) Z and (b) W^- decays.

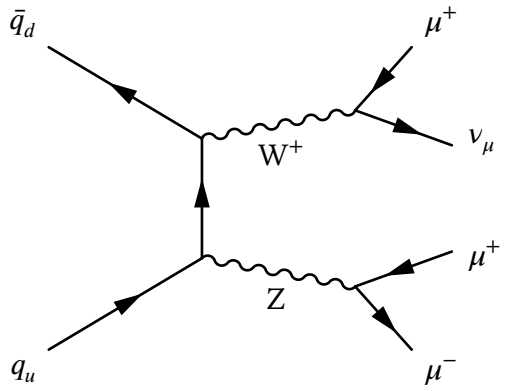

Figure 3.7: Leading order Feynman diagram for W^+Z decaying into three muons and a muon neutrino. The event contributes to the background if, for example, one of the muons, e.g. the one resulting from W^+ decay is not reconstructed.

4 The ATLAS experiment at the LHC

4.1 The Large Hadron Collider

The Large Hadron Collider (LHC) and its detectors are the culmination of more than 20 years of planning, instrumentation development and construction. The LHC accelerator ring is located near Geneva, Switzerland and is installed in a tunnel with a circumference of 26.7 km about 100 m underground. The accelerator ring is the last step of a sequence of particle accelerators originally constructed for previous CERN experiments (Proton and Super Proton Synchrotron) and is designed to accelerate the particles in its two beam pipes up to 7 TeV per beam, resulting in a center of mass (cms) energy $\sqrt{s}$ of 14 TeV. Apart from accelerating protons, the LHC also supports the acceleration of ions. At four interaction points, the two counter-rotating beams cross each other. The resulting collisions allow to draw conclusions on the involved particles and interactions by analyzing the properties of the emerging particles. Each of the four beam crossings is surrounded by a particle detector designed for a specific research purpose:

- the ATLAS detector is designed to study the physics of the Higgs boson and search for physics beyond the SM, e.g. Supersymmetry (SUSY)
- the physics program of the Compact Muon Spectrometer (CMS) is comparable to ATLAS, but employs a different detector design
- the LHCb detector is designed and optimized to study the physics of b quarks
- the ALICE detector is explicitly designed to study heavy ion collisions

One of the key aspects of the LHC is its high instantaneous luminosity of $L = 10^{-34}\,\mathrm{cm}^{-2}\,\mathrm{s}^{-1}$ at $\sqrt{s} = 14\,\mathrm{TeV}$ which is two orders of magnitude larger than the luminosities obtained with the second largest particle accelerator, the Tevatron. These unprecedented luminosities are one of the many challenges faced during the design of the LHC ring and the detectors, but allow for the study of rare physics events predicted by the SM and physics beyond the SM. After an incident involving the electrical connection between two of the superconducting magnets, the LHC is planned to operate at its design energy in 2014 after having successfully provided the detectors with stable proton beams of 3.5 TeV in 2011 and 4 TeV in 2012.

4.2 The ATLAS detector

The ATLAS (A Toroidal LHC ApparatuS) experiment is one of the four large experiments at the Large Hadron Collider (LHC) in Geneva, Switzerland. ATLAS is capable of taking data during proton-proton and heavy ion collisions of the LHC. The overall structure of the detector, shown in figure 4.1, is divided into the inner detector (ID), the calorimeter system and the muon spectrometer [2]. All sub detectors are arranged cylindrically around the beam pipe (the so-called barrels) while end caps provide sensitivity for large pseudorapidities $|\eta|$[1], i.e. $\theta \approx 0$ and $\theta \approx \pi$. ATLAS uses a right-handed coordinate system whose origin is fixed at the interaction point. The beam direction defines the z-axis and the xy-plane is transversal to the beam direction. The positive x-axis points toward the center of the LHC ring and the positive y-axis points upward. The axial angle ϕ and the polar angle θ are defined with respect to the x and z-axis.

The inner detector is the first sensitive layer and directly encloses the beam pipe. It is divided into three shells with increasing radii. The inner detector causes little energy loss to the particles traversing it and provides trajectory, momentum and particle type measurements. The silicon pixel detector is the innermost ID sub-system. It is enclosed by a silicon microstrip tracker. Both systems are used to reconstruct particle trajectories by combining single hits in the detector cells. The charge and transverse momentum p_T[2] of particles is reconstructed from the curvature of the trajectory. In addition to measurements made with the silicon trackers, the transition radiation tracker allows to distinct electron and pion tracks. The entire ID is surrounded by a superconducting solenoid which creates the axial magnetic field ($\boldsymbol{B} \approx 2\,\mathrm{T}$) necessary for the p_T and charge measurements.

The calorimeter system is separated into the electromagnetic calorimeter (ECal) and the hadronic calorimeter (HCal), which are used to measure the energy and shower shapes of the traversing particles. Both colorimeter systems are sampling calorimeters, i.e. they are segmented into passive layers which are suited to produce particle showers and active layers which measure the energy deposition due to the shower. The active material of the ECal is liquid argon and lead plates are used as passive material. The materials used for the HCal are different for the barrel and end-cap region. The tile calorimeter of the barrel uses steel and scintillating tiles. The end-cap (HEC) and forward calorimeter (FCal) both use liquid argon as the active material and copper as passive material (in addition tungsten is used in some of the FCal layers). The ECal is surrounded by the HCal as shown in figure 4.2. The great majority of particles are stopped in the calorimeter system. Due to their long lifetime, high mass and because they do not participate in the strong interaction, muons can traverse the calorimeter system. The kinematic properties of muons are measured by the muon spectrometer.

[1] Pseudorapidity is defined as $\eta = -\ln\tan\theta/2$.

[2] Transverse momentum p_T is defined as the momentum in the xy-plane, i.e. $p_T := \sqrt{p_x^2 + p_y^2}$

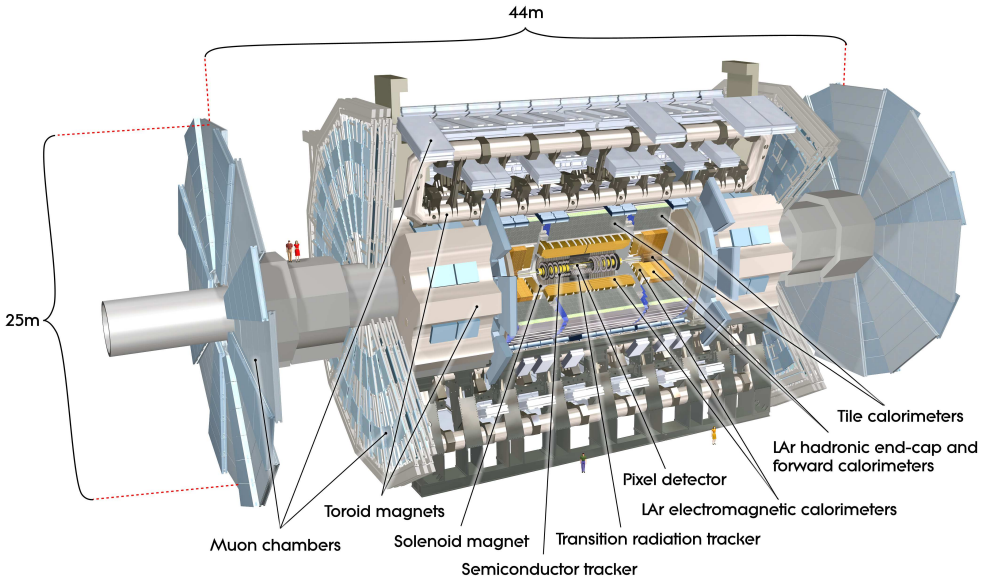

Figure 4.1: Overview of the ATLAS detector. Image source: [2]

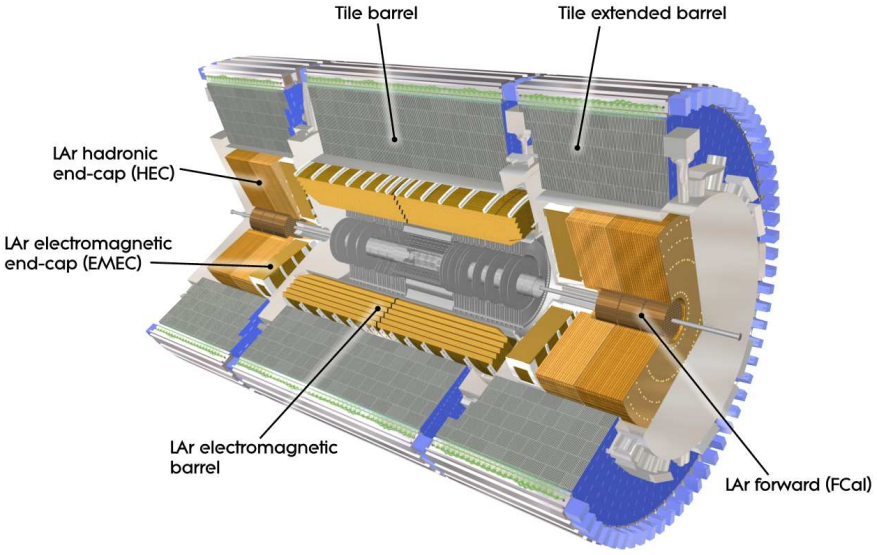

Figure 4.2: Overview of the electromagnetic and hadronic calorimeter systems of the ATLAS detector. Image source: [2]

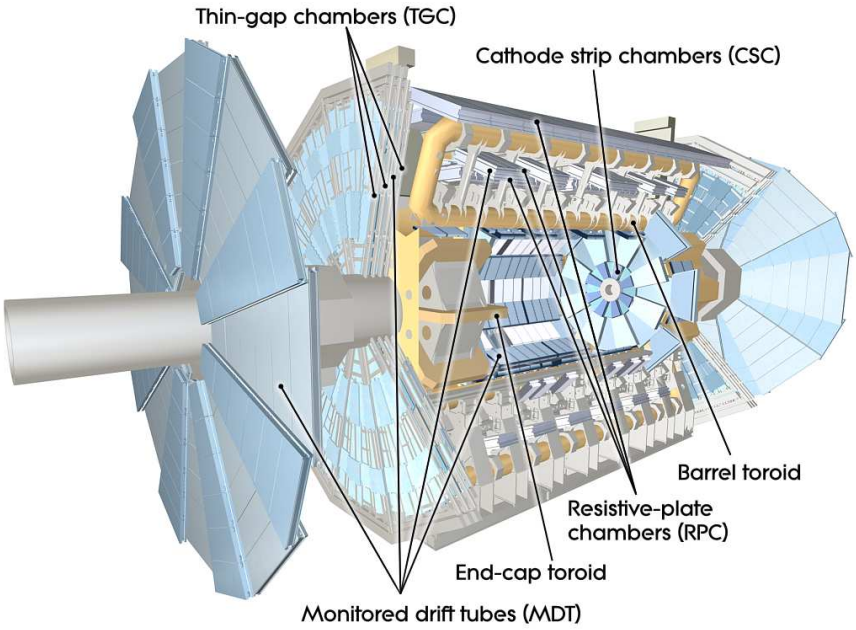

Figure 4.3: Overview of the ATLAS muon spectrometer. Image source: [2]

The ATLAS muon spectrometer (MS) is the last detector layer and provides almost 2π azimuthal coverage[3] and is sensitive for pseudorapidities $|\eta| < 2.7$. A schematic overview of the muon system is shown in figure 4.3. A toroidal magnetic field bends the muon tracks in the muon spectrometer and the resulting track curvature is used to determine p_T and p_z. The spectrometer itself is designed in three layers (inner, middle and outer). In the barrel, the layers are cylindrical about the beam pipe with increasing radii and the transverse detectors are disks with the prominent endcap wheels being the outer layer.

[3]The region about ($\eta \approx 0, \phi \approx \pi/2$) is left uncovered by the MS to allow access and feed cabling to the ID

5 Monte Carlo event generation

Any collider-based physics search uses Monte Carlo (MC) generators to simulate expected background from known SM processes as well as to simulate signal samples of the new physics to be studied. Monte Carlo techniques are employed in a twofold way:

- phase space integrators apply numeric integration techniques to solve phase space integrals to obtain cross sections
- MC generators produce physics events to be further processed into the detector simulation and event selection

Many MC event generators, often in conjunction, are in use at ATLAS and in this study. A prototypical MC production chain might start with event generation using Pythia [21] whose output (the physics events) are then processed in the ATLAS detector simulation and consequently reconstructed using the Athena framework. Athena [10] is the official ATLAS software based on the Gaudi framework [12] and handles among many other tasks:

- integration of external MC event generators for a coherent work environment
- detector simulation
- digitization of the (sub-)detector signals
- reconstruction of the physics objects from those signals
- creation of Root Ntuple files[1] used for analysis

Athena is configured via Python scripts, so-called jobOption files. The manipulations of data within the Athena software are referred to as transformations.

The SM background samples for this study, described in chapter 3, are taken from the official ATLAS MC production. Due to the immense processing and storage demands, the MC production tasks are performed on the LHC computing grid and supervised by the MC production team upon request by analysis groups to reduce redundancy of the MC samples generated for ATLAS studies. Since the MC sample contains all information for

[1] Ntuple files contain one or more data trees which organize the data of each event. Each variable, e.g. muon p_T, is stored in a branch and can be read out using C++ and the Root framework.

each event, both on truth and reconstructed level[2], the sample of a single MC production run can occupy several terabytes of storage. It is unfeasible to download such amount of data from the grid in its entirety, much less analyze it in an event selection on a reasonable timescale.

Apart from the data compression used within ROOT [22], two techniques are commonly used to reduce storage demands by creating a partial copy of the full event information:

- Slimming: physics information is removed for the event, i.e. only branches of interest are kept in the NTUPLE ROOT file
- Skimming: a basic event selection is performed, usually using a simple selection based on trigger decisions

The Slimming tool used in this study uses ATHENA built-in functionality and reduces the file size by a factor of about 6. For a list of the background samples used, see appendix chapter C.

The MCPM signal samples for this study were produced with MADGRAPH running on a conventional PC. Further event generation using PYTHIA as well as the subsequent detector simulation and the reconstruction were performed on the LHC computing grid.

5.1 MCPM signal definition and simulation chain

The MCPM exhibits two tree-level decay channels with dimuon final state which are not present in the SM: $h' \to \mu^+\mu^-$ and $h'' \to \mu^+\mu^-$ where theory requires $m_{h'} > m_{h''}$. Thus, the total cross section times branching ratio for muonic decay of the MCPM is higher compared to the SM and the invariant mass spectrum of the MCPM features two additional resonance peaks for h' and h'', provided their mass difference can be resolved. Therefore, a search for the MCPM in the dimuon channel would need to look for two resonance peaks at two unknown masses. However, the cross section times branching ratio of the decay of either MCPM Higgs boson is independent of the other and both are the same for equal masses [16]. This justifies the independent search for excesses in the dimuon invariant mass spectrum. Of course, a discovery of MCPM signature would require the observation of two new resonance peaks. For this study, the expected MCPM signal due to h' decays is simulated.

The MCPM MC event generation employs a number of programs. The MC production sequence implemented in the context of this study is illustrated in figure 5.1 and each step is discussed in the following sections.

[2]Truth level refers to the properties of MC generated events as reported by the generator, while the reconstruction level refers to the properties reported by the detector (simulation) and its particle reconstruction software.

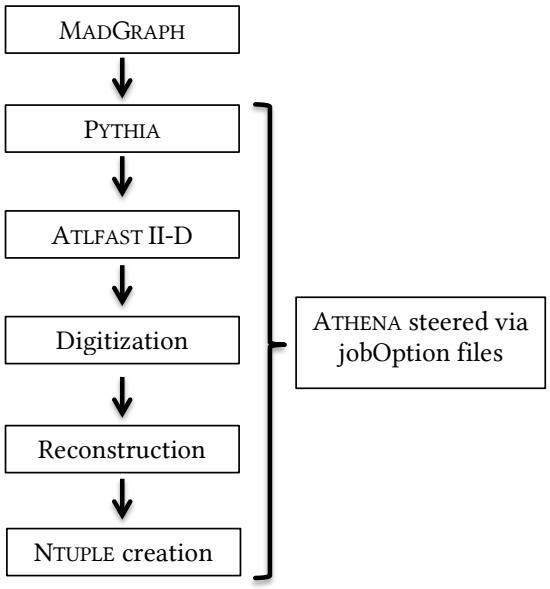

Figure 5.1: The MCPM signal event generation sequence implemented for this study. All MC production steps except MadGraph are performed within the Athena software.

5.2 Bare event generation with MadGraph

The new physics included with the MCPM, namely the MCPM Higgs bosons and their interaction with the remaining particles was implemented into MadGraph at leading order (LO) and validated in [6]. The calculation of the cross section and the generation of the $2 \to 2$ scattering events with the h' Higgs boson as an intermediary particle are performed in MadGraph and MadEvent [4] respectively. In the scope of this study, MadEvent and MadGraph are not distinguished and both are commonly referred to as MadGraph. The physics events generated by MadGraph are bare tree level events as shown in figure 5.2. Signal samples with the mass of the h' boson $m_{h'}$ set equal to 125 GeV, 150 GeV, 200 GeV, 500 GeV, 1 TeV, and 2 TeV are generated for this study. The number of events in each signal sample is 5500 and the center of mass energy is set to $\sqrt{s} = 7$ TeV. The events are encoded in the Les Houches Accord Lha format (sometimes also Lhe). A parser to extract the event information from the Lha file was written to produce the validation plots.

Figure 5.3 shows the kinematics plots of the $m_{h'} = 150$ GeV bare signal sample created by MadGraph. The invariant mass spectrum of the final state muons is shown in plot (a). The position of the resonance peak at 150 GeV and the width of the resonance agree with the validation performed in [6]. The p_T spectrum shown in plot (b) has its maximum at approximately 75 GeV, which agrees with expectation of the p_T being equally distributed among the two muons on average. The exact shape of the p_T cannot be validated due to lack of a reference spectrum, however, the suppression of very large and very low p_T

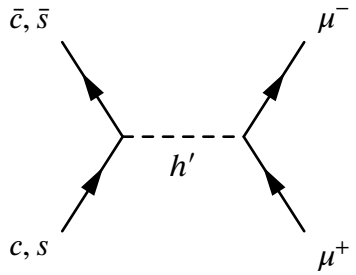

Figure 5.2: Bare event generated by MadGraph; only this hard process is included in the Lha file.

muons seems plausible. The spectrum of the leading[3] and sub-leading muon are exactly equal because of conservation of momentum in the transverse plane. The ϕ distribution shown in (c) is constant within the statistical uncertainty as predicted by the theory and validated in [6]. The η distributions of the muon with negative and positive charge are shown in plot (d) and (e) respectively. Both spectra peak at $\eta = 0$ which is expected for proton beams of equal energy. The excess due to the sensitivity of the ATLAS muon system being effectively[4] limited to $|\eta| < 2.4$ for the physics studied here, an $|\eta| < 2.5$ requirement has been set for MC generation to decrease the number of events lost during detector simulation. To compare the η spectra to the theory prediction, a Lorentz transformation into the center of mass frame is performed and the angle θ_{cms} is calculated. The theory expectation is a constant $\cos\theta_{\text{cms}}$ distribution, because the MCPM Higgs boson h' is a scalar particle [6]. However, the $|\eta| < 2.5$ requirement at event generation causes the $\cos\theta_{\text{cms}}$ distributions shown in (f) and (g) to be decreased for small $|\theta_{\text{cms}}|$. Again, conservation of momentum causes the $\cos\theta_{\text{cms}}$ spectrum of the μ^+ to be the same as the one of the μ^- reflected about 0, i.e. $\Delta\theta_{\text{cms}} = \pi$.

The tree level MCPM signal events created with MadGraph need to be extended to approximate real physics events that include not just the hard interaction, but also processes like fragmentation of the proton remnants. This is achieved with Pythia which processes the events and the MCPM physics information included in the header of the Lha file. This step is far more time consuming than the generation of bare events with MadGraph and is thus done on the LHC computing grid.

[3] Physics objects, i.e. particles and jets in the final state are ordered by p_T and referred to as leading for highest and sub-leading for second highest p_T object.

[4] The MS trigger system extends up to $|\eta| < 2.4$ and uses the trigger measurement of the ID which extends up to $|\eta| < 2.5$. Events with muons of larger η values are therefore highly unlikely to be recorded.

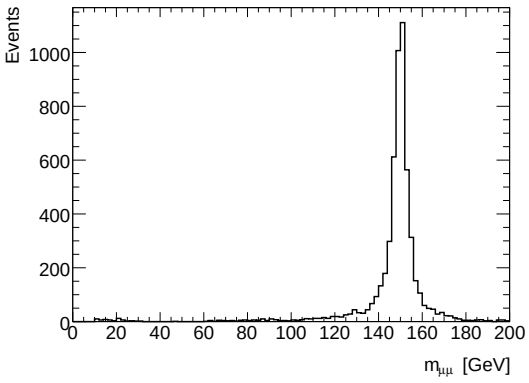

(a)

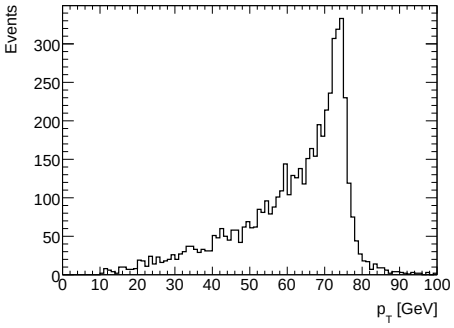

(b)

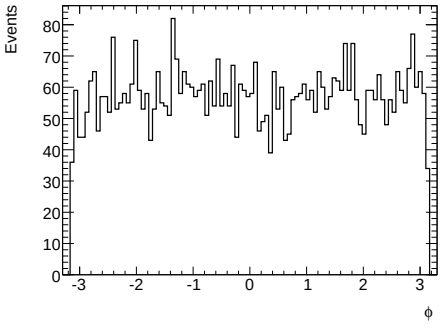

(c)

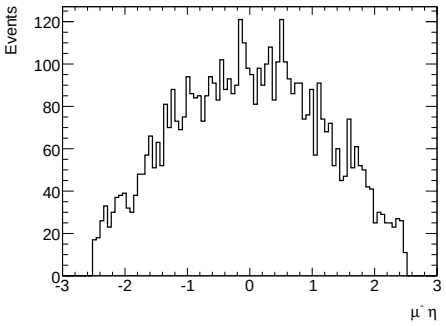

(d)

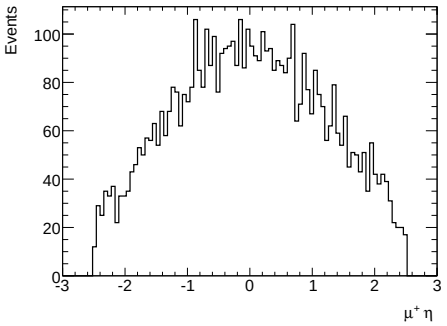

(e)

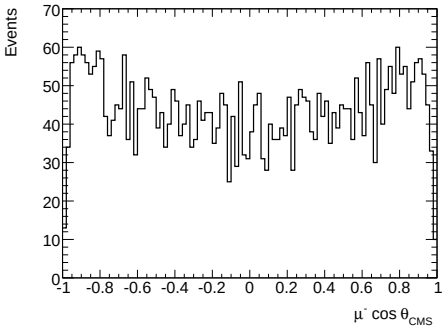

(f)

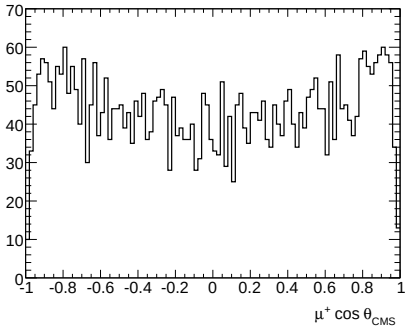

(g)

Figure 5.3: Validation plots for the $m_{h'} = 150\,\text{GeV}$ bare event sample generated with MadGraph. The total number of events is 5500.

5.3 Event generation with Pythia

The bare events generated by MadGraph do not include the plethora of accompanying processes that naturally occur in proton-proton collisions and general particle collisions. These processes are simulated and joined with the bare event to create a MC event that approximately models real proton-proton events. Pythia adds processes, including

- initial (ISR) and final state radiation (FSR)
- fragmentation of the proton remnants
- hadronization of those remnants

Figure 5.4 shows kinematic distributions of the 150 GeV signal sample after being modified by Pythia. The invariant mass spectrum is presented in plot (a), which shows minor changes to the peak height, compared to the spectrum of the bare signal. This is expected because not all bare events are processed with Pythia, but a reserve of 500 is used to avoid errors due to Pathena[5] being configured to not retry an event that has failed during execution of Pythia. The p_T spectra of the leading and sub-leading muon after full event simulation are shown in plots (b) and (c). In comparison to the bare event spectrum, both peaks are slightly shifted to lower p_T and both peaks are broader. The later is be due to Pythia adding initial state radiation resulting in initial transverse momentum of the hard process quarks. From the η distributions shown in plots (d) and (e), it becomes clear that the former stringent requirement of $|\eta| < 2.5$ is smeared out. The ϕ distributions shown in plots (f) and (g) are constant with statistical fluctuations as expected.

For the commands used to invoke Pythia within the Athena framework, see appendix chapter D. The extended events created by Pythia are stored in so-called Evgen files which are used as input for the detector simulation.

[5] Pathena is an interface to control the grid-specific algorithm parameters to run Athena on the LHC computing grid.

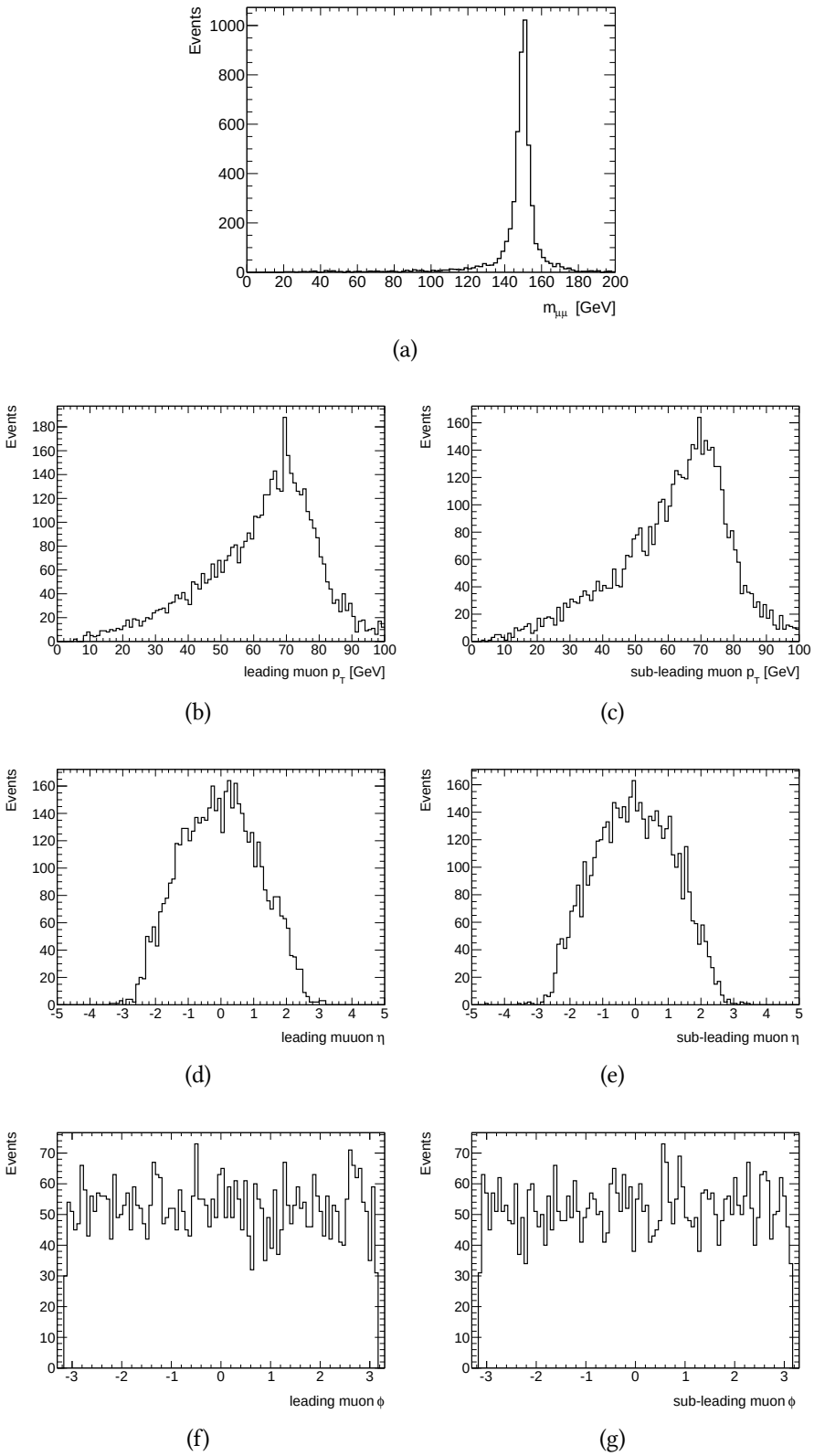

Figure 5.4: Validation plots for the $m_{h'} = 150\,\text{GeV}$ full event sample generated with Pythia. The muon with largest p_T is called the leading muon.

5.4 Detector simulation - ATLFAST II

Knowing the detector response to a given physics process is crucial to properly estimate the expected background and signal. In addition to the detector response, the geometry of the detector needs to be taken into account. Full detector coverage around the nominal interaction vertex is not possible, i.e. the geometric acceptance is limited. Dead material[6] might also influence measurements or even absorb particles entirely.

The ATLAS detector simulation is based on GEANT4 [3] and incorporates the interaction between the particles included in the EVGEN file and yields the expected energy deposition in the detector due to these interactions. Just as the event generation for the official ATLAS MC samples, this simulation is performed by the MC production team on the grid and requires the majority of processing power necessary for full MC generation, i.e. the simulation of one event taking between 10 and 15 minutes.

Due to time and computing power constraints, the ATLFAST II-D detector simulation [5] is used in this study to obtain detector signal from MCPM events. Here, only particle interactions with the inner detector are simulated in GEANT4 and all particles but muons are removed from the event upon exit of the ID. The particle interaction with the calorimeter, except for muons, are treated in the separate FASTCALOSIM simulation [5] because in the full detector simulation, more than 90% of the computing time is needed to simulate the particle interactions with the calorimeters. FASTCALOSIM uses parameterizations of particle energy response and energy distributions in the calorimeter obtained from full simulation with GEANT4 to reduce computing time. Muons and their interaction with the calorimeter and the muon system are performed in the full GEANT4 simulation. Because of this de facto full simulation of the detector response to muons, the effect of using the fast detector simulation should be negligible for this study of the dimuon final state. In addition to the generated events in the EVGEN file, the detector simulation adds minimum bias[7] MC events to the event to simulate the effect of pile-up[8]. The overall computing time compared to the full simulation is reduced by about one order of magnitude.

The output of the detector simulation are HIT files[9] that include the interactions between detector hardware and particles. These HIT files are then passed to the digitization transformation to create electrical signals of the detector hardware, which are identical to the signals produced by real events, and stores these signals in a byte stream RDO file. The electric signals of each sub detector are then used to create physics objects during the reconstruction (reco) transformation whose output are ESD (Event Summary Data) and AOD (Analysis Object Data) files. The later are subsets of the information included in

[6] The term dead material subsumes non-sensitive constituents of the detector, e.g. cabling or supporting structures

[7] Minimum bias refers to events that are not selected by a certain exclusive trigger. Minimum bias events are therefore dominated by soft interactions.

[8] High instantaneous luminosities cause multiple interactions per bunch crossing, the so-called pile-up.

[9] A detector signal is colloquially referred to as a "hit" in the detector.

the Esd files and are tailored for subsequent Ntuple creation. The transformation from Aod to Ntuple is done using a D3pd maker whose output are Root files that include data trees which organize and store physics objects and allow easy readout for analysis purposes.

The plots in figure 5.5 show the kinematics of the 150 GeV signal sample after Atlfast-II detector simulation. The number of events with at least two muons is reduced to 4793 due to the insensitive detector region at ($\eta \approx 0, \phi \approx 0$). This effect is also visible in the η distributions shown in plots (e) and (f). The invariant mass spectrum in plot (a) features the expected resonance of the h' Higgs boson.

Figure 5.6 compares the resonance peaks of all signal samples on truth and reconstructed level. The influence of the detector resolution on the signal samples with h' masses up to 200 GeV is visible, but the deviations are small. The deviations for the signal samples with $m_{h'}$ set to 500 GeV and 1 TeV are considerable. The resonance of the 2 TeV signal sample is barely visible.

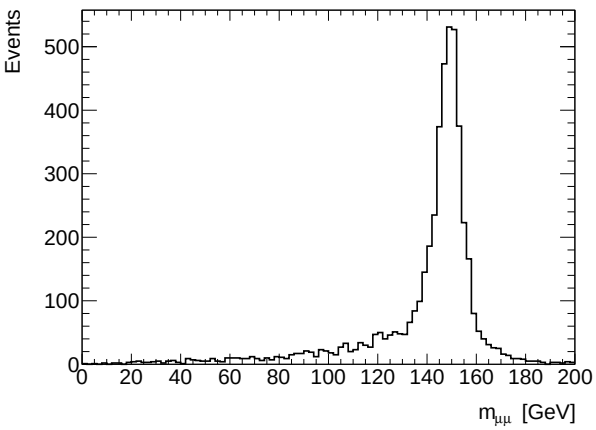

(a)

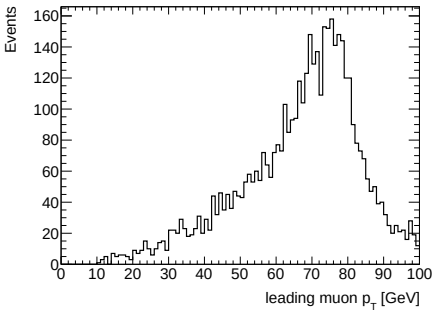

(b)

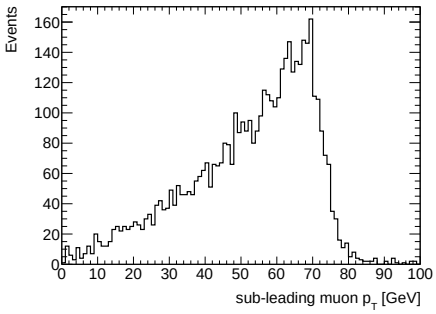

(c)

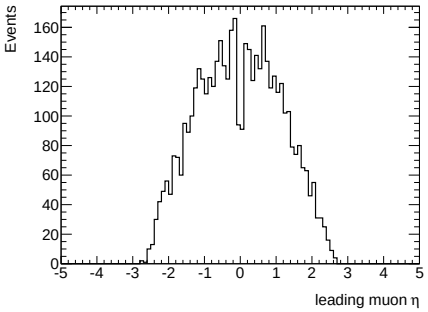

(d)

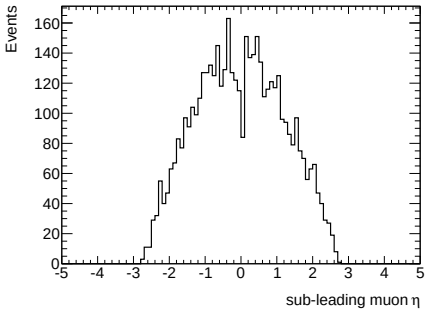

(e)

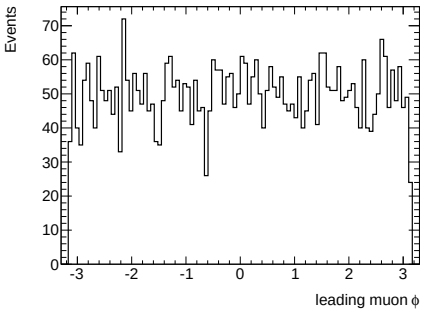

(f)

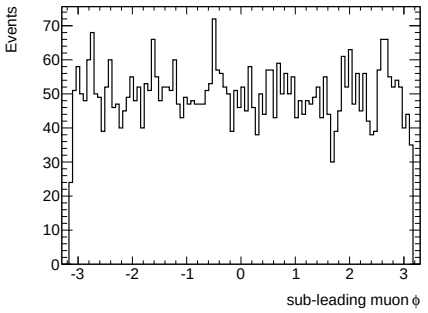

(g)

Figure 5.5: Validation plots for the 150 GeV signal sample after ATLFAST-II detector simulation.

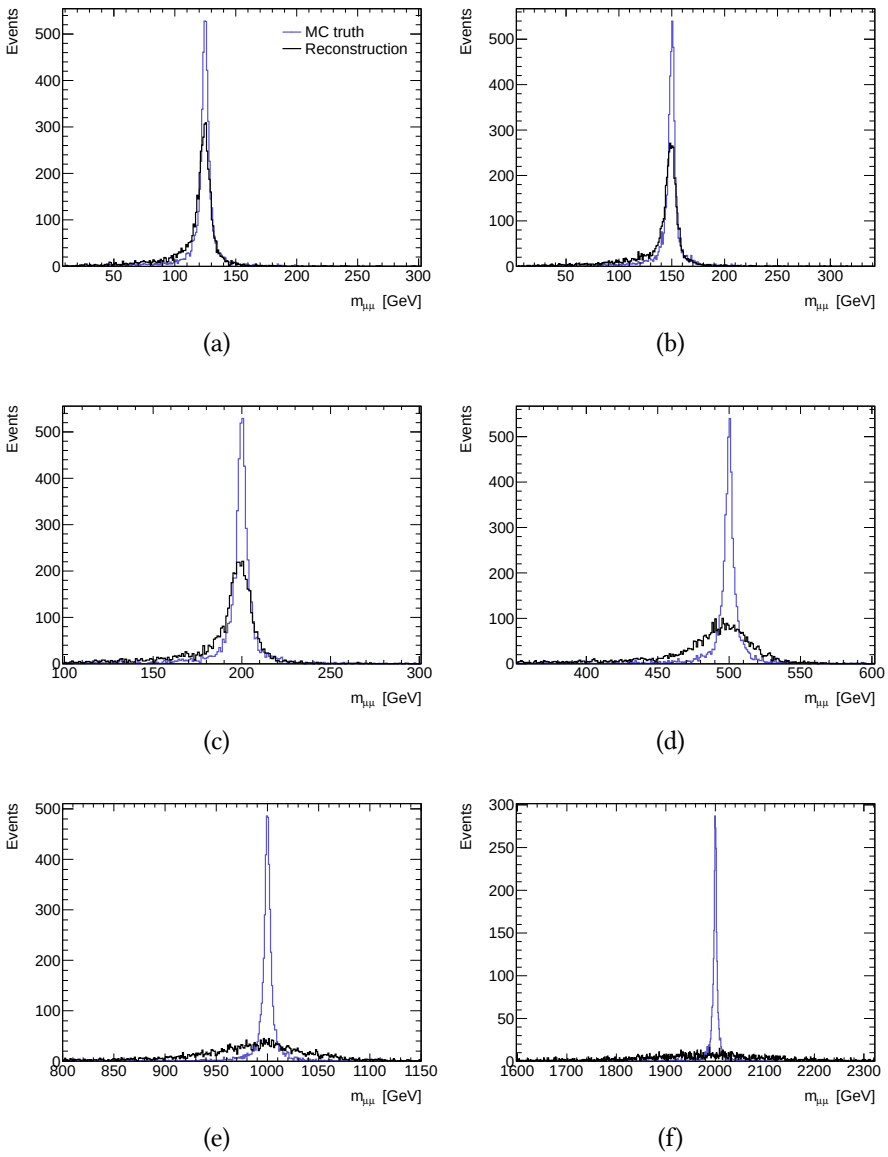

Figure 5.6: Comparison between MC truth and reconstructed invariant mass spectrum of the six MCPM h' boson mass samples. The legend of plot (a) is valid for all plots on this page. The detector resolution has little influence for the signal samples with $m_{h'}$ up to 200 GeV, but becomes considerable for the samples of 500 GeV and 1 TeV Higgs boson masses. The resonance of the 2 TeV after reconstruction is barely visible.

6 Background simulation

The discovery potential analysis presented in this study follows the well established ATLAS Z' search [1] with the same dimuon final state. Therefore, official ATLAS MC samples for the background described in chapter 3 exist and are used here. All background samples in this study are official ATLAS MC11 production samples and are run through the full detector simulation.

The dominant background for the dimuon final state is the Z/γ^* Drell-Yan process. Much smaller background contributions from $t\bar{t}$ and diboson processes are also considered in this study, whereas the background from semileptonic decays of b and c quark has been shown in [1] to be negligible. The background of jets accompanying W bosons and QCD multijet background are also neglegible.

The Drell-Yan samples are created with Pythia 6 [21] at leading order (LO). The cross section of the Drell-Yan process is then calculated to next-to-next-to-leading order (NNLO) and the ratio to the leading order cross section is used as a mass dependent QCD k-factor. Horace [8, 9] is used to calculate an electroweak k-factor which accounts for electroweak corrections including heavy gauge-bosons. Both k-factors are taken from the Z' study[1].

The $t\bar{t}$ background is simulated at next-to-leading order (NLO) by MC@NLO [11]. Multiple parton interactions are simulated with Jimmy [7] and Herwig [13] is used to simulate the remaining underlying events and parton showers. Photos [14] is employed to simulate final state radiation.

7 Dimuon resonance analysis

This analysis estimates the sensitivity of future searches for an excess in the dimuon final state above the SM background due to the decay $h' \to \mu^+\mu^-$. If the MCPM is realized in nature, the invariant mass spectrum of the dimuon pairs selected during an analysis will display an excess over the SM background at the MCPM Higgs boson mass. The event selection used in this study is based on the event selection used in the official ATLAS Z' search [1] because of the same dimuon final state. It is implemented in C++ using the ROOT framework.

7.1 Physics objects definitions

All muons used for this analysis are required to be classified as combined by the MUID algorithm[1], i.e. momentum measurements by the inner detector and the muon spectrometer can be combined into a single track.

Muons having at least three hits in each of the three muon spectrometer layers will be referred to as three station muons. Analogously, a muon detected by only two layers of the muon spectrometer will be referred to as a two station muon, if the muon was detected in regions of good detector alignment and strong toroidal fields, as defined in appendix A. Due to residual misalignment between the muonic end-caps and the barrel, muons registered by both parts of the detector are rejected.

7.2 Event selection

The purpose of the event selection is to reject background events based on their particle content, kinematics and the quality of the measurement.

Events passing the event selection need to have a minimum of two muons with opposite charge and each muon candidate must satisfy $p_T > 25\,\text{GeV}$.

Momentum resolution is increased by requiring a minimum number of hits in the inner

[1] Two muon algorithms, i.e. algorithms that combine the muon track measurements of the various sections of the MS and ID, are in use at ATLAS: STACO and MUID, the muon data created by the later are used in this analysis.

detector as indicated in [1]. A smearing on transverse momentum is applied to all MC samples to reproduce the p_T resolution in data. The p_T smearing algorithms are provided by the Muon Combined Performance group (MCP).

Muons from cosmic rays are rejected by requiring the distance along the beam-line between muon and primary vertex to be less than 1 mm. Also, the transverse impact parameter $|d_0|$ is required to be less than 0.2 mm while the z position of the primary vertex has to be within 200 mm of the detector center. Background from jets is reduced by imposing an isolation cut as follows: the sum of transverse momentum of all non-muonic tracks with $p_T > 1$ GeV in a $\Delta R < 0.3$ cone[2] around each muon μ_i is required to be less than $0.05 \cdot p_T(\mu_i)$. It is worth noting that the limited geometric acceptance of the MS gives rise to an implicit $|\eta| < 2.7$ requirement.

The exact selection criteria are:

- the event has at least one of the following boolean event filter triggers set to true: `EF_mu22` (at least one muon with $p_T \geq 22$ GeV in the event), `EF_mu22_MG` (same as `EF_mu22`, but filled by the MuonGirl algorithm), or `EF_mu40_MSonly` (at least one muon with $p_T \geq 40$ GeV in the muon spectrometer)
- at least one primary vertex with more than two associated tracks and a distance along the beam axis to the center of the detector of less than 200 mm in the event
- there are at least two muons which are marked as combined by Muid
- each muon is required to have $p_T > 25$ GeV; muon p_T smearing is applied before the selection
- each muon must pass the ID hits requirements of the Muon Combined Performance (MCP) analysis guideline as outlined in appendix A
- the impact parameter in the transverse plane with respect to the primary vertex d_0 must be less than 0.2 mm for each muon
- the impact parameter along the beam axis with respect to the primary vertex z_0 must be less than 1.0 mm for each muon
- each muon is isolated, i.e. the sum of p_T of all tracks in a $\Delta R < 0.3$ cone around each muon is less than $0.05 \cdot p_T$ of that muon
- each muon must pass requirements on MS hits and on the deviation of ID and MS momentum measurements as outlined in appendix A
- the invariant mass of the muon pair must be larger than 70 GeV

Out of the muons that passed the MS hits selection, pairs of opposite charge are formed

[2] The pseudorapidity-azimuthal angle ΔR is defined as $\Delta R = \sqrt{\Delta\eta^2 + \Delta\varphi^2}$.

if both are three station muons or if one is a two station muon and one is a three station muon. If more than one pair of muons can be selected from the event, the pair with highest sum of p_T is chosen.

The result of each selection criterion on the background and signal samples is shown in table 7.1. The number of events has been scaled to a luminosity $L = 5\,\mathrm{fb}^{-1}$.

Comparison of the number of events passing the event selection programmed for this study with the numbers reported in the Z' search reveals a small excess. It was verified that the p_T smearing implemented in this study causes about 20 additional events to pass the selection, which amounts to a discrepancy of less than 1‰. This is much smaller than the deviations due to not performing pile-up and p_T reweighing which are of the order of 3%.

The effect of each selection criterion on the background and signal samples is shown in table 7.1. Kinematics plots of the $m_{h'} = 150\,\mathrm{GeV}$ signal and the background are shown in figure 7.1.

Table 7.2 shows the number of background events and the associated statistical uncertainties for several mass bins. Comparing the uncertainties reported in [1], it becomes clear that the dominant contribution to the uncertainty is the systematic error. A full analysis of the systematic uncertainties involved in search for the MCPM goes well beyond the scope of this thesis and further treatment of uncertainties is therefore not performed.

	$m_{\mu\mu}$[GeV]				
	$110-200$	$200-400$	$400-800$	$800-1200$	$1200-3000$
$Z/\gamma*$	$21\,986 \pm 104$	2141 ± 26	177.1 ± 0.9	7.87 ± 0.04	0.947 ± 0.005
$t\bar{t}$	681 ± 5	212.6 ± 2.8	14.1 ± 0.7	0.1 ± 0.1	< 0.00001
Diboson	292 ± 3	98.3 ± 1.8	11.8 ± 0.6	0.8 ± 0.2	0.06 ± 0.05
Total	$22\,959 \pm 104$	2452 ± 26	203.1 ± 1.3	8.8 ± 0.2	1.01 ± 0.05

Table 7.2: The number of background events for various $m_{\mu\mu}$ mass bins. The errors are the statistical uncertainties.

	$m_{h'}$								
Number of events	125 GeV	150 GeV	200 GeV	500 GeV	1 TeV	2 TeV	Drell-Yan	$t\bar{t}$	Diboson
Total	366.78	226.315	99.03	3.7333	0.11656	0.00099825	4.1707e+06	447000	122505
Trigger	338.465	210.247	92.6129	3.51528	0.109147	0.000899224	2.97595e+06	120595	39235.2
Primary Vertex	334.503	207.576	91.5235	3.4772	0.107865	0.000889241	2.90524e+06	118248	38912.8
Two Combined Muons	307.948	192.141	84.0369	3.14867	0.0974208	0.000806586	2.04552e+06	44446.3	7983.03
p_T	278.679	178.925	80.8481	3.10013	0.0961387	0.000767055	1.63069e+06	8547.66	3787.48
ID Hits	270.39	174.806	78.9071	3.01352	0.0928983	0.000742498	1.58021e+06	8217.27	3680.22
d_0	270.317	174.76	78.8873	3.01352	0.0928517	0.000742498	1.57971e+06	7374.3	3670.06
z_0	269.657	174.444	78.7685	3.01128	0.0928051	0.0007417	1.57419e+06	7311.65	3662.42
Isolation	252.491	165.165	75.0845	2.8836	0.088469	0.000713349	1.46686e+06	4194.61	3333.01
MS Hits	152.507	98.6733	43.9693	1.6979	0.0538507	0.000432043	894754	2519.41	1973.07
$m_{\mu\mu} > 70\,\text{GeV}$	151.774	98.2207	43.8505	1.6979	0.0538274	0.000426652	882479	1849.77	1805.58

Table 7.1: Number of events passing each selection criterion. The luminosity is set to $L = 5\,\text{fb}^{-1}$.

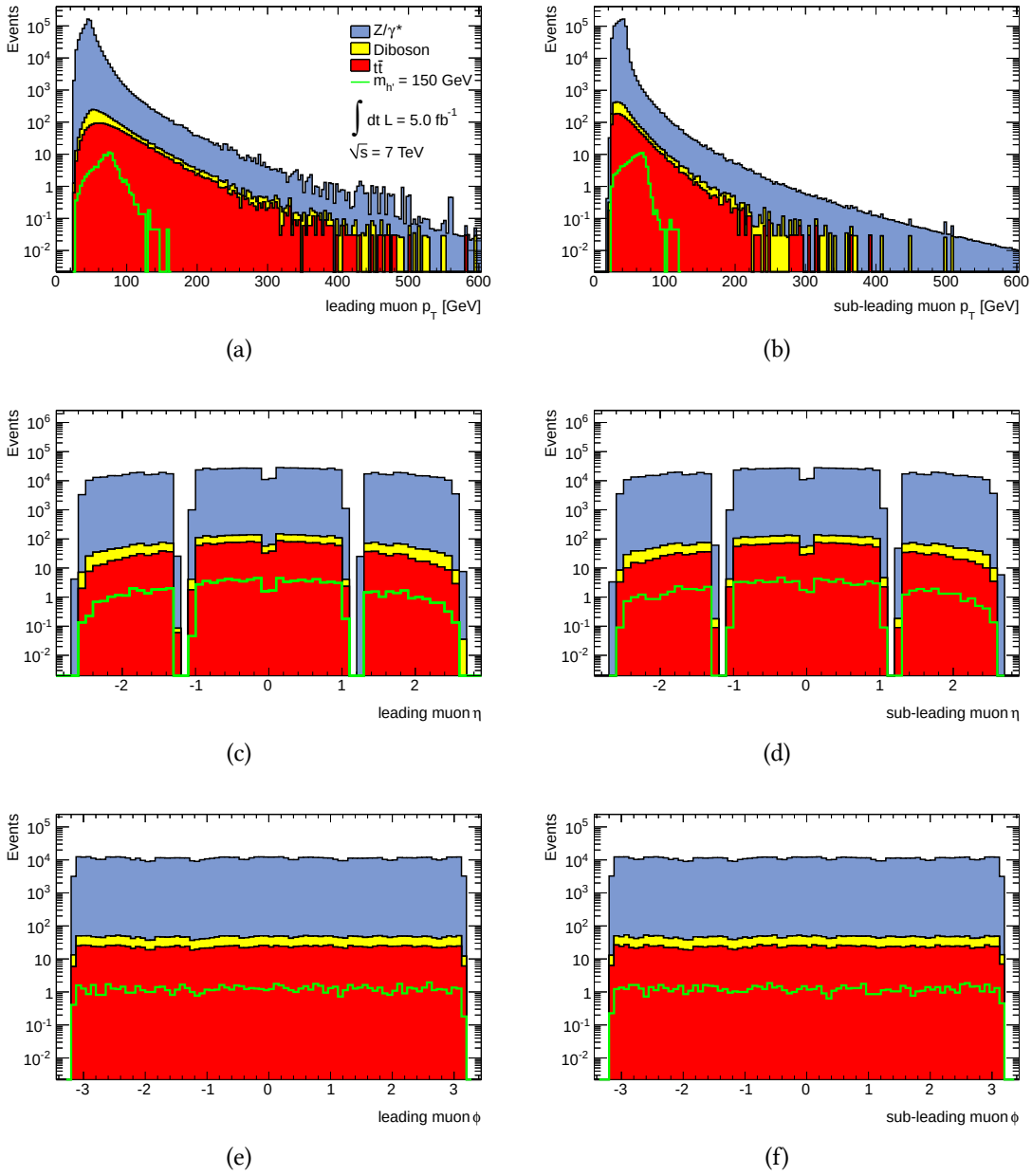

Figure 7.1: Kinematics plots of the background and the $m_{h'} = 150\,\text{GeV}$ signal sample. Plots (a) and (b) show the p_T distribution of the leading and sub-leading muon. The legend in plot (a) is valid for the remaining plots on this page. The η distribution of the leading and sub-leading muon is shown in plots (c) and (d). The decreased number of events at $\eta \approx 0$ is due to dead material (cabeling). The absence of any signal around $|\eta| \approx 1.1$ is due to the explicit exclusion of the transition region between the barrel and the end cap of the MS at $\eta = 1.05$. The azimuthal distributions are shown in plots (e) and (f).

8 Estimate of the discovery potential

The MC samples of the background and signal after event selection are scaled to a desired luminosity and the invariant mass of the selected muon pair is studied. A luminosity of $L = 5\,\mathrm{fb}^{-1}$, corresponding to the total luminosity collected during the $\sqrt{s} = 7\,\mathrm{TeV}$ collisions in 2011, is used here. Figure 8.1 shows the invariant mass distribution of the background and the enlarged signal samples. Detailed plots of the resonance peak for $m_{h'} = 125\,\mathrm{GeV}$ and $m_{h'} = 150\,\mathrm{GeV}$ are shown in figure 8.2.

The local significance of the signal n is quantified by the number of signal events S and the statistical uncertainty of the background σ_B:

$$n = \frac{S}{\sigma_B} = \frac{S}{\sqrt{B}}.$$

In this analysis, we define S and B to be the integrated number of events of the signal and the background in the $\pm\frac{1}{2}\Gamma$ region around the resonance peak. The full width at half maximum Γ is obtained by fitting a relativistic Breit-Wigner curve to the resonance as shown in figure 8.3 for the $m_{h'} = 125\,\mathrm{GeV}$ sample and in the appendix figure B.1 for the remaining signal samples.

The largest significance is found for the case of $m_{h'} = 150\,\mathrm{GeV}$, with $n = 1.28$ for $L = 5\,\mathrm{fb}^{-1}$. However, no uncertainty is assigned to the significances presented here because the systematic errors are unknown. In addition to the systematic uncertainty associated with the background, the systematic uncertainty of the signal needs to be evaluated. Both aspects go well beyond the scope of this thesis. Nevertheless, a rough estimate of the luminosities needed for discovery or exclusion of the MCPM can be made. From the significances, a luminosity independent significance factor $\gamma(m_{h'})$ is calculated

$$\gamma(m_{h'}) = \frac{S}{\sqrt{B}}\frac{1}{\sqrt{L}}$$

and used to estimate the luminosities needed to obtain a certain significance n via

$$L(n) = \left[\frac{n}{\gamma(m_{h'})}\right]^2.$$

The significance factors and the luminosities needed to obtain a given significance are shown in table 8.2 and table 8.3 respectively.

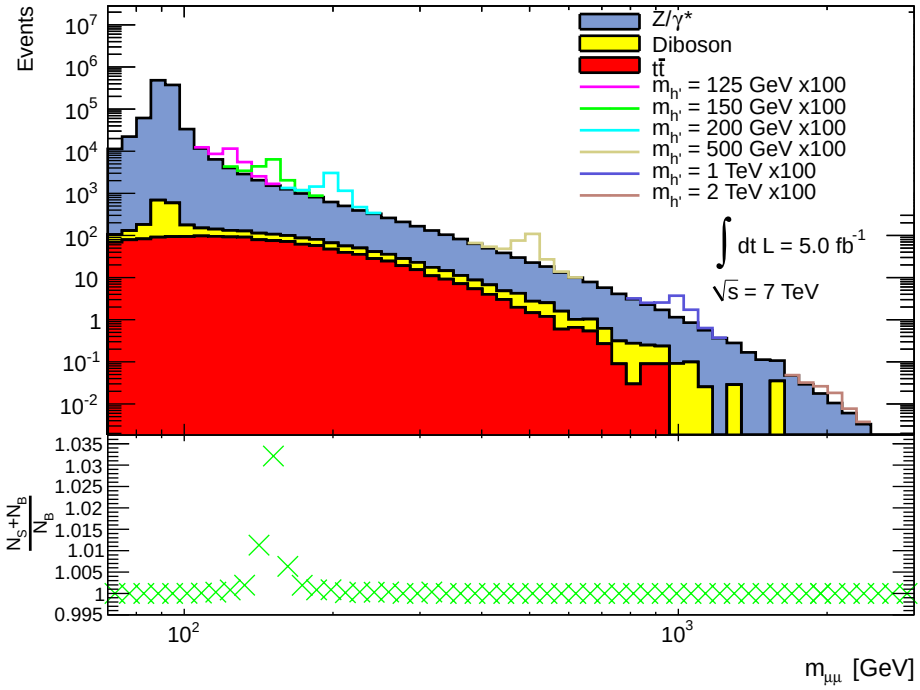

Figure 8.1: Invariant mass distribution of the muon pair after event selection. The stacked sum of the Drell-Yan, diboson, and $t\bar{t}$ background and the signals for various $m_{h'}$ are shown. The h' resonances are enlarged by a factor of 100 to make them visible. The bin width is constant in log $m_{\mu\mu}$. The bottom inset displays the ratio between the unenlarged $m_{h'} = 150\,\text{GeV}$ signal N_s plus background N_B and the background.

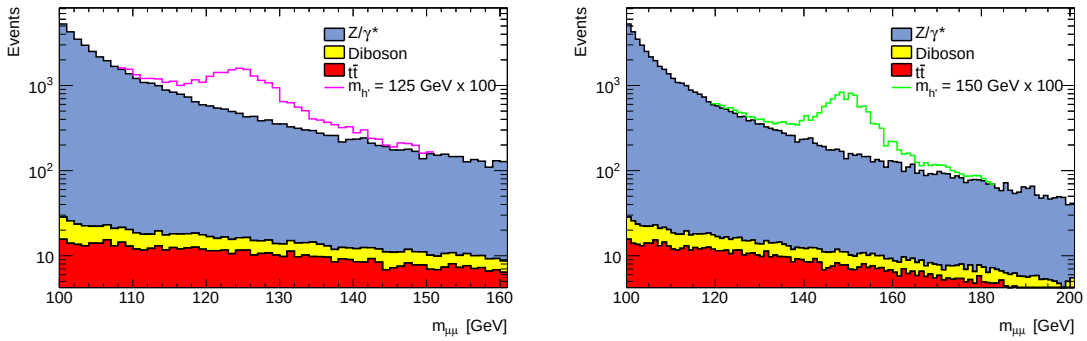

(a) (b)

Figure 8.2: Detailed invariant mass spectrum of the (a) $m_{h'}$ =125 GeV and (b) 150 GeV h' resonances.

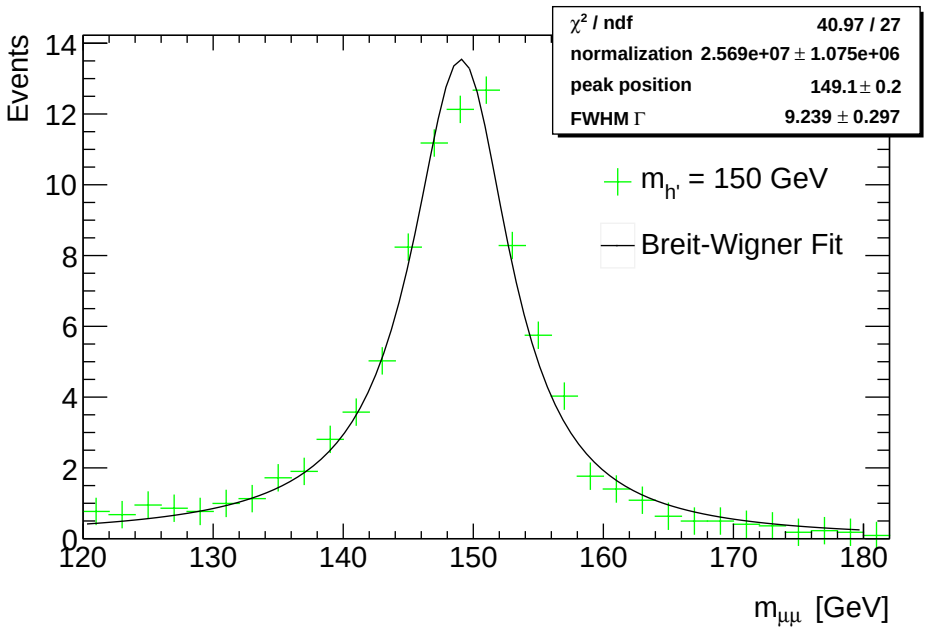

Figure 8.3: Resonance peak of the $m_{h'}$ =150 GeV signal sample with the Breit-Wigner fit function. The full width at half maximum Γ is used to define the signal region.

m_hGeV	h' signal	Z/γ^*	Diboson	$t\bar{t}$	Σ BG	n
125	108.9	7711	79.2	183.4	7974	1.22
150	70.2	2796	60.0	138.4	2994	1.28
200	32.95	1086	37.4	91.9	1215	0.95
500	1.290	39.09	2.93	2.89	44.91	0.19
1000	0.041 92	2.938	0.313	0.030	3.28	0.023
2000	$2.35 \cdot 10^{-4}$	0.3901	0.035	$< 10^{-5}$	0.425	$3.6 \cdot 10^{-4}$

Table 8.1: Number of signal and background events in the $\pm$½Γ region about the peak. The sum of backgrounds is shown in the second last and significance are shown in the last column.

	$m_{h'}$					
	125 GeV	150 GeV	200 GeV	500 GeV	1 TeV	2 TeV
$\gamma(m_{h'})$	0.55	0.57	0.42	0.086	0.010	0.00016

Table 8.2: The luminosity independent significance factors. The largest significance factor occurs for $m_{h'} = 150$ GeV.

	$m_{h'}$					
	125 GeV	150 GeV	200 GeV	500 GeV	1 TeV	2 TeV
$L[\text{fb}^{-1}]$ for 2σ	13	12	23	540	$4 \cdot 10^4$	10^8
$L[\text{fb}^{-1}]$ for 5σ	84	76	140	3400	$2 \cdot 10^5$	10^9

Table 8.3: The luminosities needed for a local significance of $n = 2$ and $n = 5$.

From the luminosities presented in table 8.3 it becomes clear that the discovery potential of the MCPM depends strongly on the Higgs boson mass. For low masses $m_{h'}$ up to 200 GeV, the $5.0\,\text{fb}^{-1}$ data collected with $\sqrt{s} = 7$ TeV collisions in 2011 and a presumed total of about $30\,\text{fb}^{-1}$ of $\sqrt{s} = 8$ TeV data that will be taken in the prolonged 2012 data taking period might be sufficient to observe first hints at the existence of the h' Higgs boson or to exclude it. The required luminosities for observation or exclusion of the existence of an h' with mass above 200 GeV are well above the integrated luminosity that will be collected until the planned shutdown of the LHC in 2013.

Apart from the event selection explicitly presented here, other selection criteria have been tested to explore possible optimizations of the luminosity independent significance factors, i.e. to further discriminate the background over the MCPM signal. A first starting point is the scalar nature of the MCPM Higgs boson h' which results in an isotropic differential cross section in the center of mass reference frame:

$$\frac{\mathrm{d}\sigma}{\mathrm{d}\cos\theta^*} = k_s = \text{const.}$$

where $\theta^* = \theta_{cms}$. The most dominant background is the Drell-Yan process which, due to the spin-1 photon and Z boson, has a differential cross section proportional to

$$\frac{\mathrm{d}\sigma}{\mathrm{d}\cos\theta^*} = k_b \cdot (1 + \cos^2\theta^*)$$

where k_b is the constant of proportionality [6]. The two muons from the decay of Z/γ^* are thus more likely to be emitted along the z-axis which could be used to separate Drell-Yan background from the MCPM signal. An additional event selection criterion based on an $|\eta|$ requirement was implemented for various η, showing an increase in the significance of less than 10%for the optimal cut-off $\eta = 2.35$. This might also be caused by low statistics. In a more elaborated search using advanced statistical techniques like a multivariate analysis, one might be able to effectively suppress the Drell-Yan background by a pseudorapidity event selection. Another discrimination criterion might be the ϕ difference between the final state muons $\Delta\phi$. The muons emitted in diboson and $t\bar{t}$ decays are less likely to have $\Delta\phi = \pi$ because the p_T of those processes is distributed among the final state muons and the accompanying particles, i.e. neutrinos for the diboson and jets from $t\bar{t}$. The normalized $\Delta\phi$ distributions of the background processes and of the h' signal are shown in figure 8.4. The $\Delta\phi$ distributions of the diboson and $t\bar{t}$ processes are not peaked around π like the Z/γ^* and MCPM h', but are increasing at an almost constant

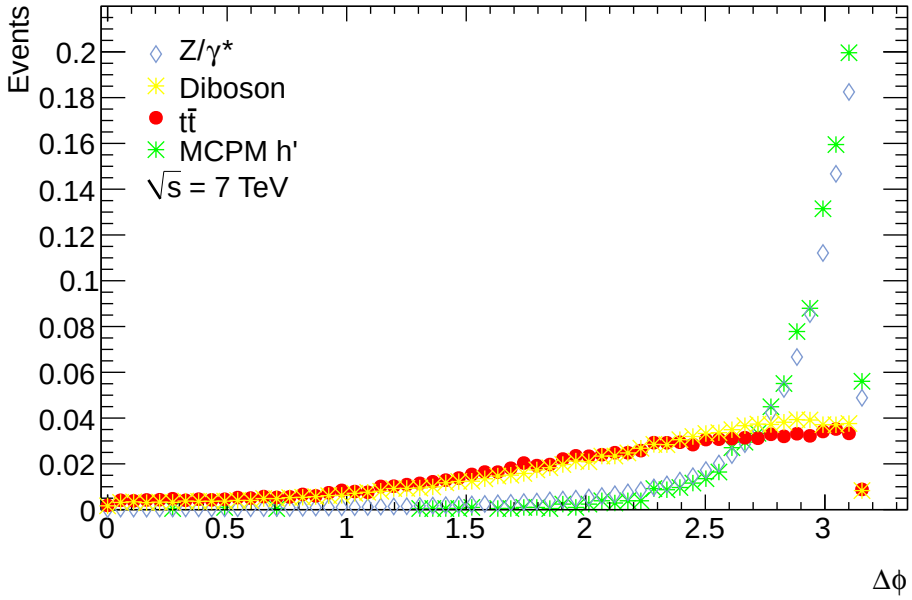

Figure 8.4: Distributions of the difference in the ϕ coordinate between the two final state muons for background and MCPM signal at $\sqrt{s} = 7$ TeV.

rate towards larger $\Delta\phi$. This might be helpful in reducing the background from diboson and $t\bar{t}$ processes. However, across the invariant mass spectrum the contribution of the Drell-Yan process is about one order of magnitude larger than the other background. As with the discrimination based on η, a more advanced search might be able to exploit this difference of background and signal.

9 Summary

The discovery potential of the maximally CP symmetric Model (MCPM) defined in [16] with the LHC ATLAS experiment was studied. Using the MadGraph implementation of the MCPM presented in [6], a complete Monte Carlo event generation chain using Pythia within the ATLAS Athena framework was implemented. The ATLAS detector response to the MCPM events was simulated using the fast detector simulation Atlfast ii-D. The Athena steering command files for the full Monte Carlo event generation chain including the detector simulation were then extended to perform these tasks on the LHC computing grid. Several signal samples of the MCPM Higgs boson h' production and decay into a dimuon final state were produced to evaluate the discovery potential of the MCPM at with the ATLAS experiment. The Standard Model background Monte Carlo samples provided by the ATLAS Monte Carlo production team were adapted for this thesis. Following the muon channel analysis of the ATLAS search for high-mass dilepton resonances [1], an event selection was programmed in C++ using Root. The results of the event selection on the background and MCPM signal was then used to estimate the luminosities needed for exclusion (2σ) and discovery (5σ) of the MCPM Higss boson h' for varying $m_{h'}$. The prolonged $\sqrt{s} = 8\,\text{TeV}$ data taking period in 2012 will yield enough luminosity to draw first conclusions on the MCPM hypothesis. Minor changes to the Athena steering commands developed for the $\sqrt{s} = 7\,\text{TeV}$ Monte Carlo event generation and detector simulation presented here will allow for the production of MCPM signal samples needed for a search at $\sqrt{s} = 8\,\text{TeV}$. The software implementation of the event selection and the automated statistics and plot creation scripts developed for this study should serve as a solid starting point for further searches on collision data. Finally, two aspects of the event topologies of signal and background have been discussed that might help improve the event selection to further suppress the background in future MCPM searches.

A MCP analysis guideline

The following selection criteria are taken from the Muon Combined Performance (MCP) group analysis guidelines. The software implementation of the spatial positions of the MS sub-detectors are also taken from the MCP.

Quoted Muon Combined Performance group ID hits requirements:

- At least one BLayer hit, if one is to be expected;
- At least 2 Pixel hits, including Pixel dead sensors crossed;
- At least 6 SCT hits, including SCT dead sensors crossed;
- At most 2 Pixel or SCT holes;
- If $\eta < 1.9$: at least 6 TRT hits, including TRT outliers, with outlier fraction < 0.9;
- If $\eta \geq 1.9$: only if at least 6 TRT hits, including TRT outliers, are observed, require the outlier fraction < 0.9

Quoted MCP group MS hits requirements for three station muons:

- At least 3 hits in all 3 layers of Barrel or Endcap Inner, Middle and Outer MDT/CSC precision layers (no Barrel-Endcap overlap);
- At least one phi hit in two different RPC/TGC/CSC layers;
- No hit in the BEE, EE or BIS78 MDT chambers;
- For each muon, the difference between the standalone momentum measurements from the ID and MS must not exceed 5 times the sum in quadrature of the standalone uncertainties

Quoted MCP group MS hits requirements for two station muons:

- At least 5 hits in both the Barrel Inner and Outer MDT precision layers (no hit in Barrel Middle layer, no Barrel-Endcap overlap)
- At least one phi hit in one RPC layer
- No hit in the BEE, EE or BIS78 MDT chambers; No hit in the MS chambers in sector 13 with $0.00 < \eta < 0.65$, or in sector 2 with $\eta > 0.85$
- For muons in large MDT sectors, $|\eta| < 0.85$; for muons in small MDT sectors, $|\eta| < 1.00$
- For each muon, the difference between the standalone momentum measurements from the ID and MS must not exceed 3 times the sum in quadrature of the standalone uncertainties.

B Results of the Breit-Wigner fits

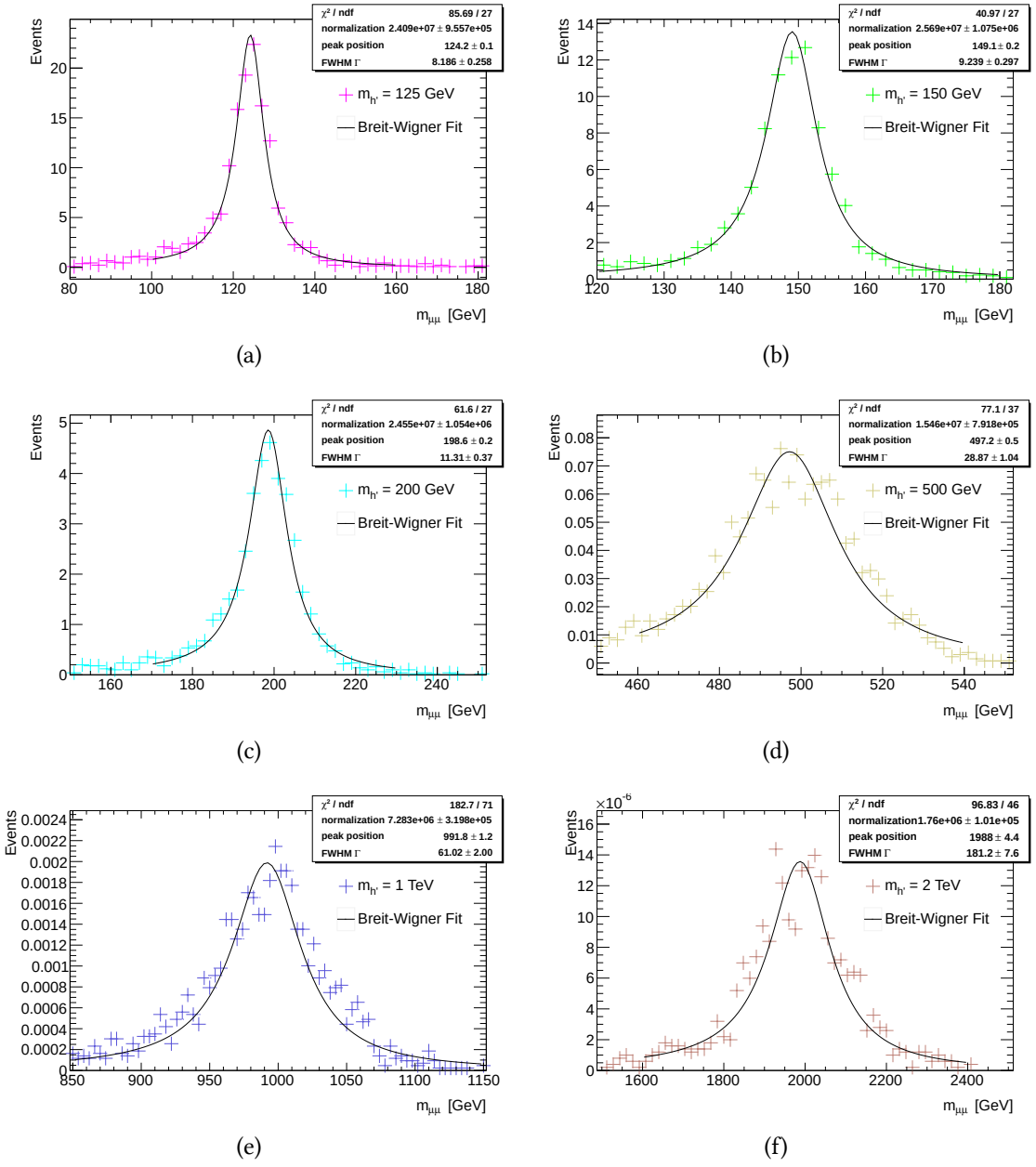

Figure B.1: Results of the Breit-Wigner Fits to the signal resonance peaks. The Luminosity is set to $L = 5\,\text{fb}^{-1}$. The fit results of the full width at half maximum (FWHM) Γ is used to define the signal region around the resonance peak.

C SM background samples

All SM background samples used for this study are official ATLAS MC production samples of the MC11 run and may be identified by their sequence of AMI (ATLAS Meta-Data Interface) tags that form the dataset name. AMI is a database storing meta information of data, MC samples and general configurations of ATHENA transformations. The AMI tags r3043 and r2993 for reconstruction and p833 for NTUP_SMWZ creation were used for all background samples.

The SM Drell-Yan background in this study consists of an inclusive sample and mass-restricted samples to improve statistics at high invariant masses. For $m_{\mu\mu} < 250\,\text{GeV}$, an inclusive sample without any mass restriction, produced with e861, s1310 and s1300 configurations for event generation and detector simulation are used. The mass restricted samples produced with the e861, s1272 and s1274 tags is used for $m_{\mu\mu} \geq 250\,\text{GeV}$used. The cross section σ_{tot} of the inclusive sample used for scaling to a desired luminosity is reduced by the $m < 250\,\text{GeV}$ cut:

$$\sigma_c = \frac{N_c}{N_{tot}}\sigma_{tot} \tag{C.1}$$

where the subscript c indicates the cross section and number of events after the $m < 250\,\text{GeV}$ cut and σ_{tot} and N_{tot} are the cross section and number of events without the cut.

The tables C.1 through C.3 show the MC channel number which allows the identification of the used MC samples.

physics process	MC number	σB [pb]	N_{events} [k]
$Z \to \mu\mu$	106047	834.6	
$Z(75,120) \to \mu\mu$	145001	798.36	100
$Z(120,250) \to \mu\mu$	145002	8.53	100
$Z(250,400) \to \mu\mu$	145003	.410	100
$Z(400,600) \to \mu\mu$	145004	.0664	100
$Z(600,800) \to \mu\mu$	145005	.01095	100
$Z(800,1000) \to \mu\mu$	145006	.002647	100
$Z(1000,1250) \to \mu\mu$	145007	.0008901	100
$Z(1250,1500) \to \mu\mu$	145008	.00023922	100
$Z(1500,1750) \to \mu\mu$	145009	.00007343	100
$Z(1750,2000) \to \mu\mu$	145010	.00002464	100
$Z(2000,2250) \to \mu\mu$	145011	.00000876	100
$Z(2250,2500) \to \mu\mu$	145012	.00000322	100
$Z(2500,2750) \to \mu\mu$	145013	.00000120	100
$Z(2750,3000) \to \mu\mu$	145014	.00000045	100
$Z(3000) \to \mu\mu$	145015	.00000025	100

Table C.1: The SM Drell-Yan background samples used in the study. The allowed Z/γ^* masses in GeV are indicated by the number in the parenthesis. The MC number is the official ATLAS MC production channel number. The calculated cross section times branching ratios are taken from the backup note to [1].

physics process	MC number	$\sigma B \times \epsilon_f$ [pb]	N_{events} [k]
$t\bar{t} \to lX$	105200	89.4	14995

Table C.2: The SM $t\bar{t}$ background sample used in the study. The MC number is the official ATLAS MC production channel number and e835, s1272 and s1274 configurations for event generation and detector simulation are used. The calculated cross section times branching ratio times filter efficiency are taken from the backup note to [1].

physics process	MC number	$\sigma B \times \epsilon_f$ [fb]	N_{events} [k]
WW	105985	17487.	249
ZZ	105986	1271.	250
WZ	105987	5743.	249

Table C.3: The SM diboson background samples used in the study. The MC number is the official ATLAS MC production channel number and e825, s13010 and s1300 configurations for event generation and detector simulation are used. The calculated cross section times branching ratio times filter (1 lepton) efficiency are taken from the backup note to [1].

D Signal sample generation code

The generation of the bare event signal sample is done in MadGraph using the commands:

```
import modelname MCPM -modelname
generate p p > h1 > m+ m-
launch
```

The output is a Lha file which is then passed to Pathena, which is an Athena version optimized for submitting jobs to the grid. The bare events are modified by Pythia. The minimum number of events per Evgen file produced with Pathena is set to 5000, smaller numbers causing errors. Pythia is called via:

```
pathena --trf "
\\athena commands:
Generate_trf.py ecmEnergy=7000 runNumber=000001 firstEvent=0
maxEvents=5000 randomSeed=13 jobConfig=MGtoPythia.py
outputEVNTFile=%OUT.root.1 inputGeneratorFile=filename._00001.tar.gz"
\\options for the grid job:
\\name of the output dataset:
--outDS oname.EVGEN
\\specify archive that includes the LHA file:
--extFile filename._00001.tar.gz
\\ grid sites needs to host pile-up files:
--site FZK-LCG2_DATADISK
\\sorts output according to filetype
\\necessary for following transformation:
--individualOutDS
\\specify athena version to be used:
--athenaTag AtlasProduction,16.6.7.13
```

Content of `MGtoPythia.py`:

```
from AthenaCommon.AlgSequence import AlgSequence
topAlg = AlgSequence("TopAlg")
```

```
include ( "MC11JobOptions/MC11_PythiaAUET2B_CTEQ6L1_Common.py" )
"pyinit pylisti -1", "pyinit pylistf 1","pyinit dumpr 1 2",
# "pydat1 parj 90 20000", # Turn off FSR.
 "pydat3 mdcy 15 1 0"   # Turn off tau decays.
]
## ... Tauola
include ( "MC11JobOptions/MC11_Tauola_Fragment.py" )
## ... Photos
include ( "MC11JobOptions/MC11_Photos_Fragment.py" )

#from GeneratorFilters.GeneratorFiltersConf import PhotonFilter
#topAlg += PhotonFilter()
#
#PhotonFilter = topAlg.PhotonFilter
#PhotonFilter.Ptcut = 10000.
#PhotonFilter.Etacut = 2.7
#PhotonFilter.NPhotons = 1
#
#from GeneratorFilters.GeneratorFiltersConf import LeptonFilter
#topAlg += LeptonFilter()
#
#LeptonFilter = topAlg.LeptonFilter
#LeptonFilter.Etacut = 2.7
#
#StreamEVGEN.RequireAlgs +=  [ "PhotonFilter" ]
#StreamEVGEN.RequireAlgs += [ "LeptonFilter" ]
#--------------------------------------------------------------
# Configuration for EvgenJobTransforms
#--------------------------------------------------------------
from MC11JobOptions.MadGraphEvgenConfig import evgenConfig
evgenConfig.inputfilebase='filneame_00001.tar.gz'
evgenConfig.efficiency = 0.9
from AthenaCommon.AppMgr import ServiceMgr as svcMgr
svcMgr.MessageSvc.OutputLevel = INFO
svcMgr.MessageSvc.infoLimit = 100000
```

The fast detector simulation is invoked using:

```
pathena --trf "AtlasG4_trf.py
conditionsTag=OFLCOND-SDR-BS7T-05-17
physicsList=QGSP_BERT
```

```
preInclude=SimulationJobOptions/preInclude.FastIDKiller.py
inputEvgenFile=%IN outputHitsFile=%OUT.hit maxEvents=500
skipEvents=%SKIPEVENTS randomSeed=%RNDM:23
geometryVersion=ATLAS-GEO-18-01-03_VALIDATION"
--inDS filename.EVGEN_EXT0/
--outDS filename.HIT
--nEventsPerFile 5000
--nEventsPerJob 500
--individualOutDS
--athenaTag AtlasProduction,16.6.7.13
```

Reconstruction and digitization are performed using:

```
pathena --trf "DigiMReco_trf.py inputHitsFile=%IN
outputRDOFile=%OUT.RDO.pool.root
outputESDFile=%OUT.ESD.pool.root
outputAODFile=%OUT.AOD.pool.root
maxEvents=500 skipEvents=0 digiSeedOffset1=%RNDM:100
digiSeedOffset2=%RNDM:100 DataRunNumber=-1 jobNumber=0
numberOfHighPtMinBias=0.045336 numberOfLowPtMinBias=39.954664
LowPtMinbiasHitsFile=%LOMBIN HighPtMinbiasHitsFile=%HIMBIN
conditionsTag=OFLCOND-SDR-BS7T-05-22 geometryVersion=ATLAS-GEO-18-01-01
postExec_h2r='ToolSvc.LArAutoCorrTotalToolDefault.NMinBias=0;
svcMgr.StatusCodeSvc.AbortOnError=False'
preExec_h2r='from Digitization.DigitizationFlags import digitizationFlags;
digitizationFlags.overrideMetadata+=[\"SimLayout\",\"PhysicsList\"]'
postInclude_h2r=FastSimulationJobTransforms/jobConfig.AtlfastIID.py,
FastSimulationJobTransforms/jobConfig.FastCaloSim_ID_cuts.py,
FastSimulationJobTransforms/jobConfig.egamma_lateral_shape_tuning.config19.py
preInclude_h2r=SimulationJobOptions/preInclude.PileUpBunchTrains2011
Config8_DigitConfig.py,RunDependentSimData/configLumi_mc11b.py,
FastSimulationJobTransforms/jobConfig.v14_Parametrisation.py
preExec_r2e='rec.Commissioning.set_Value_and_Lock(True);
jobproperties.Beam.energy.set_Value_and_Lock(3500*Units.GeV);
muonRecFlags.writeSDOs=True;
jobproperties.Beam.numberOfCollisions.set_Value_and_Lock(8.0);
jobproperties.Beam.bunchSpacing.set_Value_and_Lock(50)'
preExec_e2a='TriggerFlags.AODEDMSet=\"AODSLIM\";
rec.Commissioning.set_Value_and_Lock(True);
jobproperties.Beam.energy.set_Value_and_Lock(3500*Units.GeV);
muonRecFlags.writeSDOs=True;
jobproperties.Beam.numberOfCollisions.set_Value_and_Lock(8.0);
jobproperties.Beam.bunchSpacing.set_Value_and_Lock(50)'
```

```
triggerConfigByRun='{180164:\"MCRECO:DB:TRIGGERDBMC:308,134,246\",
183003:\"MCRECO:DB:TRIGGERDBMC:308,134,246\",186169:\"MCRECO:DB:
TRIGGERDBMC:308,134,246\",189751:\"MCRECO:DB:TRIGGERDBMC:310,139,252\"}'"
--inDS filename.HIT_EXT0/
--outDS filename.AOD
--nFilesPerJob=1
--nFiles=10
--lowMinDS
mc11_7TeV.108118.Pythia8_minbias_Inelastic_low.merge.HITS.e816_s1299_s1303/
--highMinDS
mc11_7TeV.108119.Pythia8_minbias_Inelastic_high.merge.HITS.e848_s1299_s1303/
--nLowMin 4 --nHighMin 4 --athenaTag AtlasProduction,17.0.5.1
```

Final reconstruction and NTUPLE generation:

```
pathena --trf "Reco_trf.py inputAODFile=%IN
outputNTUP_SMWZFile=%OUT.NTUP.root
maxEvents=20000 skipEvents=0
autoConfiguration=everything"
--inDS filename.AOD_EXT2/
--individualOutDS
--outDS filename.NTUP_SMWZ
--athenaTag AtlasProduction,17.0.5.1
```

E Bibliography

[1] Search for high–mass dilepton resonances with 5 fb^{-1} of pp collisions at $\sqrt{s} = 7$ TeV with the ATLAS experiment. (ATLAS-CONF-2012-007), Mar 2012.

[2] G. Aad et al. The ATLAS Experiment at the CERN Large Hadron Collider. *JINST*, 3: S08003.

[3] S. Agostinelli et al. GEANT4: A Simulation toolkit. *Nucl.Instrum.Meth.*, A506: 250—303, 2003.

[4] Johan Alwall, Michel Herquet, Fabio Maltoni, Olivier Mattelaer, and Tim Stelzer. MadGraph 5 : Going Beyond. *JHEP*, 1106:128, 2011.

[5] Coll ATLAS, M Beckingham, M Duehrssen, E Schmidt, M Shapiro, M Venturi, J Virzi, I Vivarelli, M Werner, S Yamamoto, and T Yamanaka. The simulation principle and performance of the atlas fast calorimeter simulation FastCaloSim. Technical Report ATL-PHYS-PUB-2010-013, CERN, Geneva, Oct 2010.

[6] Johann Brehmer. Monte-carlo event Generation for a Two-Higgs-Doublet Model with Maximal CP symmetry. 2012.

[7] J.M. Butterworth, Jeffrey R. Forshaw, and M.H. Seymour. Multiparton interactions in photoproduction at HERA. *Z.Phys.*, C72:637—646.

[8] C.M. Carloni Calame, G. Montagna, O. Nicrosini, and A. Vicini. Precision electroweak calculation of the production of a high transverse-momentum lepton pair at hadron colliders. *JHEP*, 0710:109, .

[9] C.M. Carloni Calame, G. Montagna, O. Nicrosini, and A. Vicini. Precision electroweak calculation of the charged current Drell-Yan process. *JHEP*, 0612:016, .

[10] The ATLAS collaboration. The ATLAS simulation infrastructure.

[11] Stefano Frixione and Bryan R. Webber. Matching NLO QCD computations and parton shower simulations. *JHEP*, 2002(06):029, 2002.

[12] G. Barrand et al. GAUDI - A software architecture and framework for building HEP data processing applications. *Computer Physics Communications*, 140(1-2):45 — 55, 2001. ISSN 0010-4655.

[13] G. Corcella et al. Herwig 6: an event generator for hadron emission reactions with interfering gluons (including supersymmetric processes). *JHEP*, 0101(2001):010—103, January 2001.

[14] Piotr Golonka and Zbigniew Was. PHOTOS Monte Carlo: A Precision tool for QED corrections in Z and W decays. *Eur.Phys.J.*, C45:97--107, 2006.

[15] Particle Data Group. Review of Particle Physics. *J. Phys. G*, 33:1+, 2006. URL `http://pdg.lbl.gov`.

[16] M. Maniatis and O. Nachtmann. On the phenomenology of a two-Higgs-doublet model with maximal CP symmetry at the LHC. *JHEP*, 0905:028.

[17] M. Maniatis, A. von Manteuffel, and O. Nachtmann. A New type of CP symmetry, family replication and fermion mass hierarchies. *Eur.Phys.J.*, C57:739—762.

[18] O. Nachtmann. *Phänomene und Konzepte der Elementarteilchenphysik*. Vieweg, 1986. ISBN 9783528089269.

[19] S.F. Novaes. Standard model: An Introduction. *hep-ph/0001283*, 1999.

[20] PDG. http://pdg2.lbl.gov/atlasblog/wp-content/uploads/2010/04/Picture-1.png.

[21] Torbjorn Sjostrand, Stephen Mrenna, and Peter Z. Skands. PYTHIA 6.4 Physics and Manual. *JHEP*, 0605:026.

[22] The ROOT team. The ROOT Users Guide 5.21. 2008.

[23] J.W.F. Valle. Neutrino physics overview. *J.Phys.Conf.Ser.*, 53:473--505.

Acknowledgements

Many people have supported me during the course of this project and I have truly enjoyed learning and working with the combined ATLAS/ILC group at KIP. Without my ever-patient counselor and teacher Sahill Poddar, the work presented here would not have been possible. I am grateful for the guidance and support of Dr. Rainer Stamen, who also helped steering this project into the right direction. The analysis software framework developed by Veit Scharff was essential to the quick progress of this project and I have greatly profited from his expertise in physics and ATLAS. The programming done for this thesis also profited from Valerie Lang, who was kind enough to let me use her analysis as a starting point for the event selection. Finally, I would like my supervisor Prof. Dr. Hans-Christion Schultz-Coulon who gave me the opportunity to work in the KIP ATLAS group and, in the process, gaining a first insight into the great ATLAS experiment.

Erklärung

Ich versichere, dass ich diese Arbeit selbstständig verfasst und keine anderen als die angegebenen Quellen und Hilfsmittel benutzt habe.

Heidelberg, den 16. Juli 2012,